Inhibitors of the V_0 subunit of the vacuolar H^+-ATPase prevent segregation of lysosomal- and secretory-pathway proteins

Jacqueline A. Sobota[1], Nils Bäck[2], Betty A. Eipper[1] and Richard E. Mains[1,*]

[1]Neuroscience Department, University of Connecticut Health Center, Farmington, CT 06030, USA
[2]Department of Anatomy, Institute of Biomedicine, University of Helsinki, FIN-00014, Helsinki, Finland
*Author for correspondence (mains@uchc.edu)

Accepted 28 July 2009
Journal of Cell Science 122, 3542-3553 Published by The Company of Biologists 2009
doi:10.1242/jcs.034298

Summary

The vacuolar H^+-ATPase (V-ATPase) establishes pH gradients along secretory and endocytic pathways. Progressive acidification is essential for proteolytic processing of prohormones and aggregation of soluble content proteins. The V-ATPase V_0 subunit is thought to have a separate role in budding and fusion events. Prolonged treatment of professional secretory cells with selective V-ATPase inhibitors (bafilomycin A1, concanamycin A) was used to investigate its role in secretory-granule biogenesis. As expected, these inhibitors eliminated regulated secretion and blocked prohormone processing. Drug treatment caused the formation of large, mixed organelles, with components of immature granules and lysosomes and some markers of autophagy. Markers of the *trans*-Golgi network and earlier secretory pathway were unaffected. Ammonium chloride and methylamine treatment blocked acidification to a similar extent as the V-ATPase inhibitors without producing mixed organelles. Newly synthesized granule content proteins appeared in mixed organelles, whereas mature secretory granules were spared. Following concanamycin treatment, selected membrane proteins enter tubulovesicular structures budding into the interior of mixed organelles. shRNA-mediated knockdown of the proteolipid subunit of V_0 also caused vesiculation of immature granules. Thus, V-ATPase has a role in protein sorting in immature granules that is distinct from its role in acidification.

Supplementary material available online at
http://jcs.biologists.org/cgi/content/full/122/19/3542/DC1

Key words: Ammonium chloride, Autophagy, Bafilomycin A1, Concanamycin A, Fusion, Regulated secretion

Introduction

Acidification of intracellular organelles is crucial to the function of the secretory and endocytic pathways. The vacuolar H^+-ATPases (V-ATPases) are responsible for establishing and maintaining intracellular pH gradients across specialized organellar membranes, including the *trans*-Golgi network (TGN), secretory granules, endosomes and lysosomes. Progressive acidification of the regulated secretory pathway is important for proteolytic processing of prohormones (Seidah et al., 1993; Seidah and Prat, 2002) and aggregation of soluble protein content (Colomer et al., 1996). Receptor-mediated endocytosis and degradation pathways also require a pH gradient (Forgac, 1999; Stevens and Forgac, 1997). The V-ATPases generate the proton-motive driving force for secondary transport processes, such as neurotransmitter uptake into synaptic vesicles (Hediger et al., 2004; Parsons, 2000), and have been implicated in the maintenance of copper homeostasis (Madsen and Gitlin, 2008).

V-ATPases are multisubunit complexes organized in two domains. The peripheral V_1 domain is composed of eight different subunits (A-H), and is responsible for catalyzing ATP hydrolysis (Morel, 2003; Nishi and Forgac, 2002; Schoonderwoert and Martens, 2001; Weimer and Jorgensen, 2003). This in turn, drives proton translocation through the V_0 domain, an integral membrane complex composed of multiple copies of the proteolipid subunits (c and c′, also called b and f) and single copies of the remaining subunits (a, d and c″) (Beyenbach and Wieczorek, 2006; Forgac, 2007; Marshansky and Futai, 2008). The closely related macrolide antibiotics bafilomycin A1 (BafA1) and concanamycin A (ConA) inhibit the V-ATPase at nanomolar concentrations by binding to the proteolipid subunit (Bowman and Bowman, 2002; Forgac, 2007; Huss et al., 2002); subunit a might also participate in binding (Wang et al., 2005). At these low concentrations, BafA1 and ConA are highly specific for V-ATPases (Bowman et al., 1988; Drose et al., 1993). Because of their specificity, these inhibitors have been widely used in studies of V-ATPase mediated acidification (Schoonderwoert et al., 2000; Taupenot et al., 2005).

The V_1 and V_0 domains, which are separately transported down axons, also function independently (Morel, 2003; Schoonderwoert and Martens, 2001). For example, the V-ATPase has been implicated in membrane fusion events; by interacting with another V_0 sector on apposing membranes, V_0 may constitute a homomeric fusion pore (Baars et al., 2007; Morel, 2003; Peters et al., 2001; Weimer and Jorgensen, 2003). The interaction of V_0a1 with the vSNARE VAMP2 and with SNARE complexes involved in vesicle docking and fusion places the V_0 portion of the V-ATPase at a strategic location for the formation of an exocytotic fusion pore (Morel et al., 2003). Moreover, V_0a1 interacts with plasma membrane tSNAREs in *Drosophila* and is required for evoked synaptic vesicle exocytosis (Hiesinger et al., 2005). *Caenorhabditis elegans* V_0a1 acts in parallel with SNARE proteins to mediate apical secretion of Hedgehog-related proteins from exosomes (Liegeois et al., 2006). Mutant mice lacking the a3 isoform, which is targeted to the membranes of insulin granules in

pancreatic β-cells, have reduced levels of plasma insulin and an impaired response to glucose (Sun-Wada et al., 2006). Similarly, vacuolar fusion in yeast requires V_0, but not pump activity, whereas fission requires pump activity (Baars et al., 2007).

We previously used ammonium chloride to study the role of acidification in sorting of soluble secretory-granule content proteins (Sobota et al., 2006). NH_4Cl and methylamine are weak bases that partition into acidic compartments, neutralizing the pH within these organelles and blocking much of intragranular endoproteolytic processing. Although no noticeable effect on secretory protein localization was observed with NH_4Cl or methylamine treatment, nanomolar concentrations of the V-ATPase inhibitors BafA1 or ConA, which caused a similar increase in lumenal pH, caused a profound and selective disruption of secretory-granule protein localization. Since these inhibitors bind to the V_0 domain of the V-ATPase, it is speculated that they disrupt the interaction of V_0 subunits with SNARE proteins (Bayer et al., 2003; Hiesinger et al., 2005; Morel et al., 2003). In the current study, we distinguish the effects of BafA1 and ConA on the regulated secretory pathway related to blockade of acidification versus those that are not mimicked by deficits in proton pumping.

Results

Localization of secretory-granule content proteins is disrupted by ConA or BafA1, but not by an increase in granule pH

Acidification of immature secretory granules by the V-ATPase has a key role in granule biogenesis. This ATPase can be blocked with specific inhibitors, or the pH gradient it establishes can be dissipated. We found that these two approaches had similar effects on granule pH (supplementary material Figs S1 and S2), but vastly different effects on secretory-granule morphology in AtT-20 corticotrope tumor cells (Fig. 1). In control cells, confocal imaging demonstrated partial colocalization of an exogenous secretory-granule content protein (PHM-GFP) and endogenous proopiomelanocortin (POMC) products. Punctate structures were found throughout the cell, with some staining detectable in the region of the Golgi complex (Fig. 1A) (Sobota et al., 2006). Dissipation of the pH gradient by NH_4Cl and methylamine treatments (supplementary material Fig. S1A, Fig. S2) had no discernible effect on the punctate structures containing PHM-GFP and POMC products (Fig. 1B).

By contrast, cells treated with a low dose of ConA (Fig. 1C) or BafA1 (supplementary material Fig. S1B) for 24 hours contained very few morphologically normal secretory granules. Both PHM-GFP and POMC products accumulated in large, round structures located in the region adjacent to the Golgi or TGN (Fig. 1C, arrowheads). Despite this striking alteration in localization of PHM-GFP and POMC, the Golgi complex was unaffected; the pattern of GM130 staining was identical in cells treated with either ConA or vehicle (Fig. 1, right, blue). A few secretory granules of normal size were seen at the margins of the ConA-treated cells (Fig. 1C, arrows).

Three methods were used to assess granule pH. Acridine orange visualization and DAMP staining confirmed that both NH_4Cl and ConA treatment obliterated intracellular pH gradients (supplementary material Fig. S1A). To provide a more quantitative assessment of granule pH, the GFP variant pHluorin (Miesenbock et al., 1998), whose fluorescence intensity is pH sensitive, was targeted to granules by fusion to a secretory-granule protein and stably expressed in AtT-20 cells (supplementary material Fig. S2). Based on live-cell imaging fluorescence intensity, exposure of PHM-pHluorin AtT-20 cells to ConA, NH_4Cl or methylamine raised secretory-granule pH above pH 7.0 within 15 minutes; pH was maintained between 7.15 and 7.27 for at least 24 hours by all three drugs. Importantly, despite the major changes in cell morphology, these drug effects were largely reversed 8 hours after drug removal (supplementary material Fig. S1C) and fully reversed after 16-24 hours; cells exposed to these low doses of drug did not undergo apoptosis.

Formation of the large structures containing PHM-GFP and POMC was dependent on both drug concentration and treatment time. When lower concentrations or shorter incubations with either ConA or BafA1 were used, the structures were smaller; an increase in diameter was observed with longer incubations or higher concentrations of drug (data not shown). Since ConA and BafA1 have similar effects, whereas neutralization of the pH gradient to a similar extent with NH_4Cl or methylamine does not, our data indicate a unique role for the ConA- or BafA1-sensitive component(s) of the vacuolar ATPase in secretory-granule formation. A role for the V-ATPase in membrane fusion events involved in the exocytosis of synaptic vesicles (Hiesinger et al., 2005) and exosomes (Liegeois et al., 2006) in the balance of vacuolar fusion and fission in

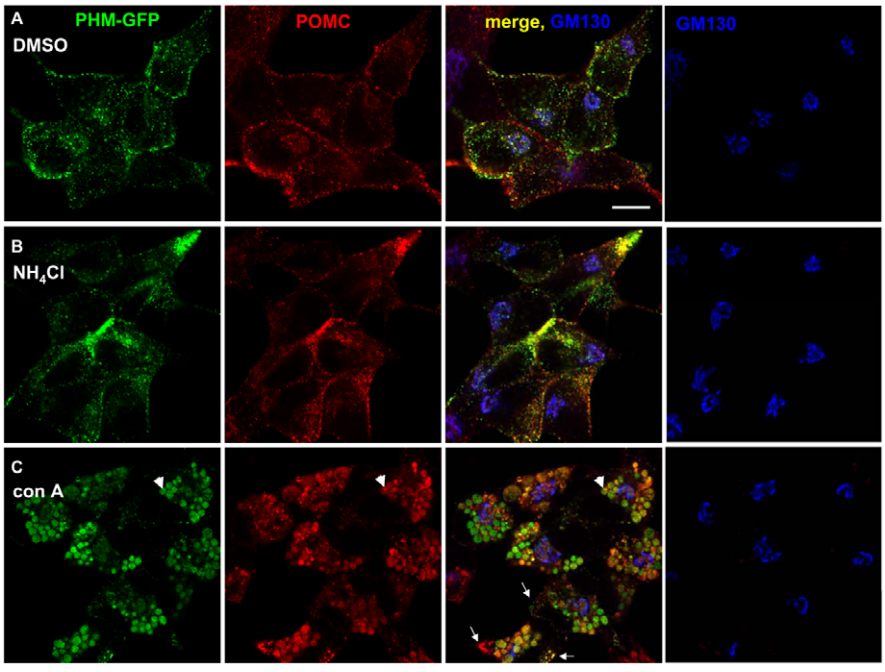

Fig. 1. Ammonium chloride and ConA have different effects on secretory protein localization. AtT-20 cells stably expressing PHM-GFP were treated overnight with growth medium containing 0.00001% DMSO, 2.5 mM NH_4Cl or 1 nM ConA in 0.00001% DMSO. Fixed cells were permeabilized and visualized with a rabbit polyclonal antibody to ACTH that recognized ACTH biosynthetic intermediate, ACTH and CLIP (red). Golgi stacks were visualized simultaneously using a mouse monoclonal antibody against GM130 (blue). A few normal secretory granules remain after ConA treatment (arrows), along with large mixed organelles (arrowheads). Scale bar: 10 μm.

yeast (Baars et al., 2007) and in protein sorting (Forgac, 2007; Marshansky and Futai, 2008), led us to consider similar roles for V-ATPase early in the regulated secretory pathway.

ConA induces formation of mixed organelles containing secretory-granule and lysosomal proteins

To pursue this possibility, the composition of the enlarged, PHM-GFP-positive structures formed as a result of ConA or BafA1 treatment was analyzed. We first examined several other soluble secretory-granule proteins, including chromogranin A and prohormone convertase 1 (PC1). Both proteins accumulated in these large vesicular structures (supplementary material Fig. S3A,B). Since the V-ATPase is also responsible for acidifying the interior of lysosomes, we evaluated the effect of ConA on localization of lysosomal-associated membrane protein-1 (LAMP-1), an integral membrane protein, and cathepsin B, a soluble component of lysosomes (Fig. 2A,B). Secretory granules and lysosomes were easily distinguished in control PHM-GFP cells (Fig. 2A,B, left). In ConA-treated cells, LAMP-1 staining surrounded the PHM-GFP-positive structures and cathepsin B, similarly to PHM-GFP, was located in the interior of these structures (Fig. 2A,B, right).

Effects of ConA on other cell types

To determine whether these results were unique to AtT-20 cells, GH3 cells expressing PHM-GFP were subjected to the same treatment. ConA treatment resulted in the formation of large, round PHM-GFP-positive vesicles in GH3 somatomammotropes (supplementary material Fig. S4A). LAMP-1 also surrounded the large PHM-GFP-positive vesicles that form in ConA-treated GH3 cells (supplementary material Fig. S4A, arrowheads). Although secretory granules are unique to neuroendocrine cells, lysosomes are not. We therefore evaluated the effect of ConA on lysosomes in NIH 3T3 cells (supplementary material Fig. S4B). Visualization of endogenous LAMP-1 in cells expressing EGFP revealed a heterogeneous collection of lysosomes concentrated in the perinuclear region. ConA treatment produced large LAMP-1-positive structures that excluded cytosolic GFP (arrowhead); lack of soluble protein markers makes exclusion of GFP the best marker for these structures. The ability to produce these large vesicles in response to ConA treatment is not unique to neuroendocrine cells. The large vesicular structures formed in response to ConA are ‘mixed’ organelles. Interestingly, PC12 cells were the only cell type examined that did not show formation of mixed organelles in response to prolonged ConA treatment; localization of LAMP-1, PHM-GFP (supplementary material Fig. S4C) and chromogranin B (not shown) were unchanged compared with control PC12 cells.

Secretory-granule membrane proteins are in the interior of mixed organelles

We next asked how secretory-granule membrane proteins responded to ConA treatment. For this experiment, AtT-20 cells stably expressing PAM-2 fused to GFP (PAM-2-GFP) were analyzed after fixation. In control cells, most of the PAM-2-GFP was present in punctate, vesicular structures; some colocalization with syntaxin-6, a TGN marker, was also apparent (Fig. 2C). Very little overlap of PAM-2-GFP with LAMP-1 was observed. In fixed ConA-treated cells, PAM-2-GFP was found in the LAMP-1-positive mixed organelles (Fig. 2C); the irregular pattern observed within these mixed organelles suggests that membranes containing PAM-2-GFP entered their interior (Fig. 2C, inset). Very little PAM-2-GFP was present on the cell surface.

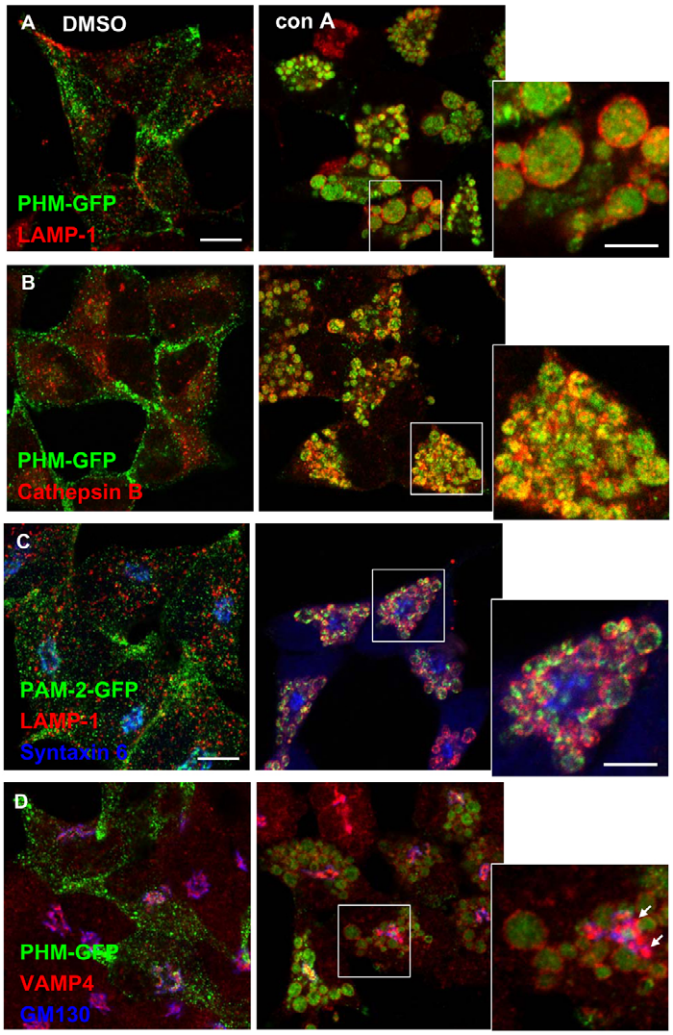

Fig. 2. Characterization of structures formed by ConA treatment. After fixation and permeabilization (in pH 7.4 buffer), lysosomal proteins LAMP-1 (A) and cathepsin B (B) were visualized along with PHM-GFP in control cells and in AtT-20 cells subjected to the ConA paradigm. (C) Syntaxin-6 and LAMP-1 were visualized simultaneously in ConA-treated and control AtT-20 cells expressing PAM-2-GFP, a membrane protein. (D) VAMP4 and GM130 were visualized simultaneously in ConA-treated and control AtT-20 cells expressing PHM-GFP. Arrows indicate clusters of VAMP4-positive structures. Scale bars: 10 μm (left), 5 μm (inset).

VAMP4 normally localized to the TGN and immature secretory granules (Fig. 2D, left), and is removed during secretory-granule maturation and acquisition of regulatory competence (Eaton et al., 2000). As observed for LAMP-1, the mixed organelles formed in response to ConA treatment were outlined by a VAMP4-positive membrane; VAMP4 staining is not seen within the mixed organelles. VAMP4 staining within the TGN does not retain its normal tubuloreticular morphology; VAMP4-positive structures are clustered, as if aggregated (Fig. 2D, inset, arrows).

To try to identify the structures affected by ConA, we examined several Golgi and TGN markers. Staining for adaptor proteins AP1, AP2 and AP3 demonstrated that none of these was associated with the mixed organelles (supplementary material Fig. S5). AP1-positive structures accumulated between the mixed organelles whereas AP2-positive structures were concentrated along the plasma membrane; AP3 localization was unaltered. Staining for TGN38 was unaffected

(supplementary material Fig. S5C, blue). These results suggest a remarkably selective effect of ConA on selected post-TGN compartments, immature granules and lysosomes.

Endocytosis is blocked by ConA

Acidification by the V-ATPases is known to have an essential role in endocytic trafficking. This is particularly important in receptor-mediated endocytosis, because a low pH in early endosomes can trigger dissociation of ligand-receptor complexes (Forgac, 1999). Because secretory-granule membrane proteins undergo endocytosis following release of soluble granule proteins, we chose to assess the effects of ConA on endocytic trafficking in AtT-20 cells expressing PAM-1, an integral membrane form of PAM that undergoes extensive luminal cleavage in AtT-20 cells. As seen for PAM-2-GFP, the majority of the PAM-1 moved from the TGN area to the limiting membrane of the mixed organelles and structures within this limiting membrane following ConA treatment (Fig. 3A,B). Control and ConA-treated AtT-20 PAM-1 cells were allowed to take up anti-PAM antibody for a brief time. In control cells, the internalized PAM antibody was present in small vesicular structures throughout the cytoplasm; the distribution of internalized PAM antibody was not dramatically altered by ConA treatment (Fig. 3A).

Following a brief incubation with fluorescently tagged transferrin, control PAM-1 AtT-20 cells are filled with transferrin-containing vesicular structures, some of which were positive for EEA1 (Fig. 3B). Very few of these structures contained membrane PAM. Unlike membrane PAM, endocytosis of transferrin was completely blocked by a 24 hour pretreatment with ConA; transferrin was present only on the cell surface (Fig. 3B). The steady state localization of EEA1 was not disrupted by ConA treatment, indicating that this endocytic compartment is not targeted for inclusion in the mixed organelles.

ConA blocks stimulated secretion of cargo proteins

Progressive acidification of the luminal compartment is essential for PC1 maturation (Schmidt and Moore, 1995). Since ConA and NH_4Cl have similar effects on luminal pH (supplementary material Fig. S2), they should have similar effects on the post-TGN, autocatalytic conversion of 82 kDa PC1 into 67 kDa PC1 (Zhou and Mains, 1994). Consistently with this, both treatments reduced the cell content of 67 kDa PC1ΔC (supplementary material Fig. S6A).

Processing and secretion of POMC, which begins in the TGN and occurs primarily in secretory granules (Schnabel et al., 1989), was evaluated with an antibody directed against γMSH. In control cells, intact POMC and the 16 kDa fragment were the major products stored (supplementary material Fig. S6B). Although processing of POMC into 16 kDa fragment was largely eliminated by ConA treatment, the level of 16 kDa fragment in the cells was hardly affected by NH_4Cl (supplementary material Fig. S6B), methylamine or chloroquine treatment (Mains and May, 1988). All treatments diverted much of the intact POMC into the medium under basal conditions (supplementary material Fig. S6B).

We next evaluated the effect of both ConA and NH_4Cl on regulated secretion of PHM-GFP. Following pretreatment for 24 hours with vehicle, ConA or NH_4Cl, basal secretion and $BaCl_2$-stimulated secretion were monitored over 30 minute collection periods and cell lysates were prepared. PHM-GFP in medium and cell extracts was quantified by enzymatic assay. In both control and NH_4Cl-treated cells, $BaCl_2$ elicited robust secretion of PHM-GFP (supplementary material Fig. S6C). Secretion was not significantly stimulated by $BaCl_2$ following ConA treatment. The large, mixed organelles formed in response to ConA treatment were not responsive to secretagogue, but disrupting pH gradients with NH_4Cl had a negligible effect on secretion.

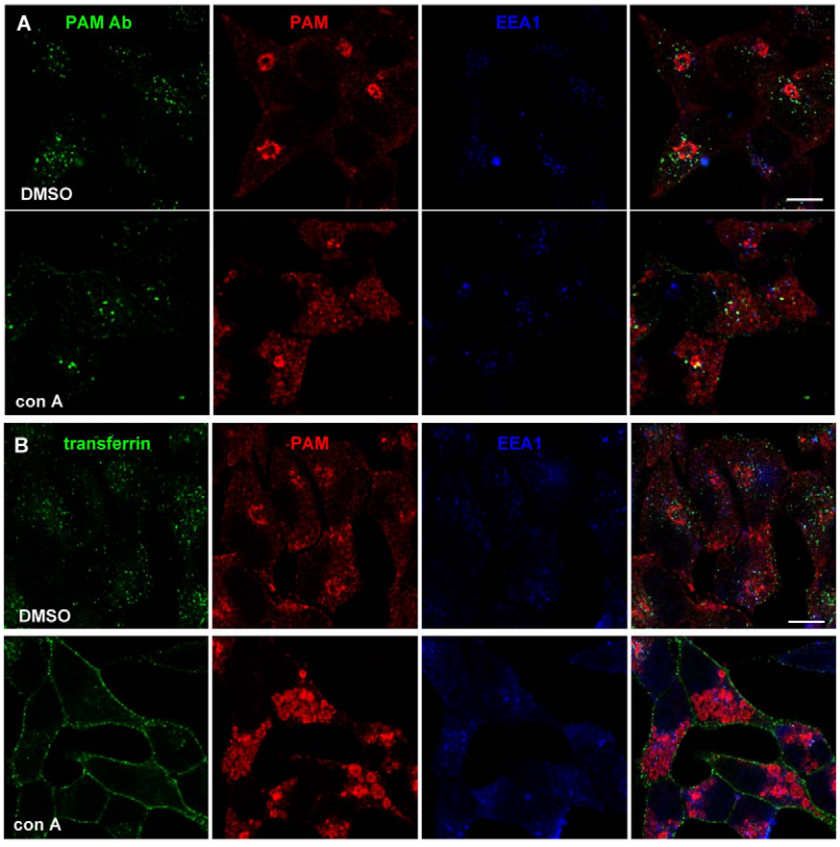

ConA causes invagination into vacuoles near the TGN

Transmission electron microscopy was used to explore the identity of the mixed organelles; cells were fixed after 2-24 hours of treatment with 10 nM ConA (Fig. 4). The higher dose was selected for these studies because the effects are more pronounced at short times, when the primary effect of the drug should be most apparent. The first effect seen after 2 hours of treatment was the appearance of 300-600 nm vacuoles in the *trans*-Golgi area (Fig. 4B, arrow); control cells lacked similar structures (Fig. 4A). These vacuoles generally

Fig. 3. Internalized transferrin and internalized PAM antibody do not enter mixed organelles. AtT-20 PAM-1 cells exposed to vehicle or ConA were allowed to internalize PAM luminal domain antibody for 20 minutes (A) or labeled transferrin for 10 minutes (B). Cells were then rinsed, fixed and permeabilized. (A) Internalized PAM antibody (green) was visualized along with the cytosolic domain of PAM (red) and early endosome marker EEA1 (blue). (B) The luminal domain of PAM-1 (JH629; red) was visualized along with internalized transferrin (green) and the early endosome marker EEA1 (blue). PAM-1 is cleaved into soluble, luminal domain fragments which are secreted and integral membrane cytosolic domain fragments which undergo endocytosis; as a result, antisera to the luminal domain visualize secretory granules better, while cytosolic domain antisera highlight the TGN and endocytic pathway. Scale bars: 10 μm.

appeared empty; in some vacuoles, invagination of vesicles approximately 50 nm in diameter could be seen (Fig. 4B, arrow). Based on membrane apposition, these vacuoles appeared to fuse with enlarged lysosomes (Fig. 4C, arrows). Mixed organelles, containing lysosomal structures and accumulations of 50 nm vesicles were formed (Fig. 4D, arrowheads), and images showing mixed organelles apposed to lyososomes suggest continued fusion (Fig. 4E, arrows).

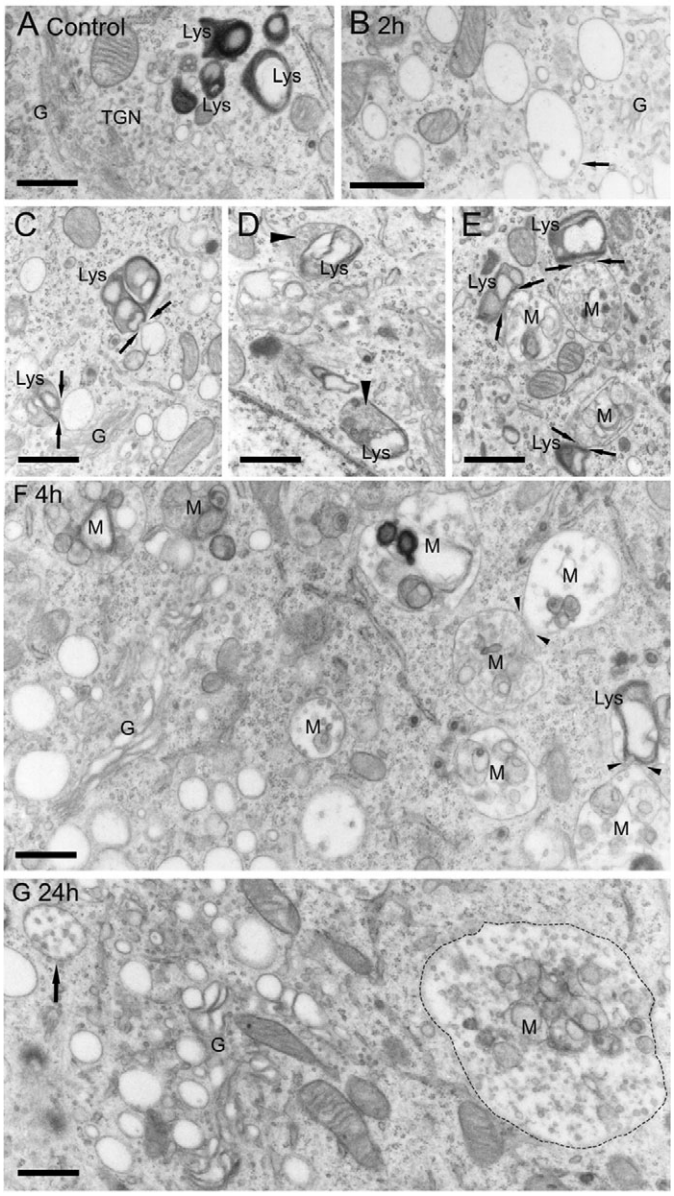

Fig. 4. Examination of biogenesis of mixed organelles using electron microscopy. (A) The TGN in AtT-20 cells expressing membrane PAM-1 is a tubuloreticular structure. Lysosomes (Lys) have a distinct morphology. (B) After 2 hours in 10 nM ConA, vacuoles appeared in the TGN; most were empty, with some showing inward vesiculation (B, arrow). Vacuoles appeared to fuse with lysosomes (C, arrows), forming organelles with distinct lysosomal and vesicular regions (D, arrowheads). Mixed organelles (M) continued to fuse with lysosomes (E, arrows). (F) After 4 hours in ConA, mixed organelles were more common; fusion to lysosomes was still observed (arrowheads). (G) After 24 hours, the mixed organelles were larger; smaller vesicle-containing vacuoles were still observed in the *trans*-Golgi area (arrow). Scale bars: 0.5 μm.

After 4 hours of ConA treatment (Fig. 4F), normal lysosomes were no longer seen. Lysosomal features could still be distinguished in the mixed organelles. The vacuolar structures were often closely connected (Fig. 4F, arrowheads). After 24 hours of treatment the mixed organelles were larger (dotted line), contained more internal vesicles and no longer contained structures resembling normal lysosomes (Fig. 4G). The Golgi stack remained intact and empty vacuoles could still be seen in the *trans*-Golgi area, suggesting their continued formation.

To confirm the role of fusion in the formation of large mixed organelles, lysosomes were labeled by incubating PAM-1-GFP cells with TRITC-dextran for 1 hour followed by an overnight chase. Time-lapse confocal microscopy following the addition of 10 nM ConA revealed the fusion of pre-existing lysosomes with PAM-1-GFP-positive structures to form mixed organelles within 1 hour of drug treatment (supplementary material Fig. S7).

Secretory-granule membrane proteins enter internal vesicles

One of the first observable responses to ConA is the appearance of TGN-associated vacuoles with several internal vesicles. We used immunoelectron microscopy to ask whether membrane proteins normally associated with immature secretory granules (PAM) or lysosomes (LAMP-1) and endosomes (mannose-6-phosphate receptor) appeared in these internal vesicles. To explore the initial accumulation of membrane proteins in TGN-associated vacuoles, we treated cells with a low dose of ConA (1 nM) for 2 hours (Fig. 5). Vacuolization of the TGN was apparent, and electron-dense material was often associated with the invaginations and internal vesicles. The morphology of multivesicular bodies (MVB) was not affected (Fig. 5A).

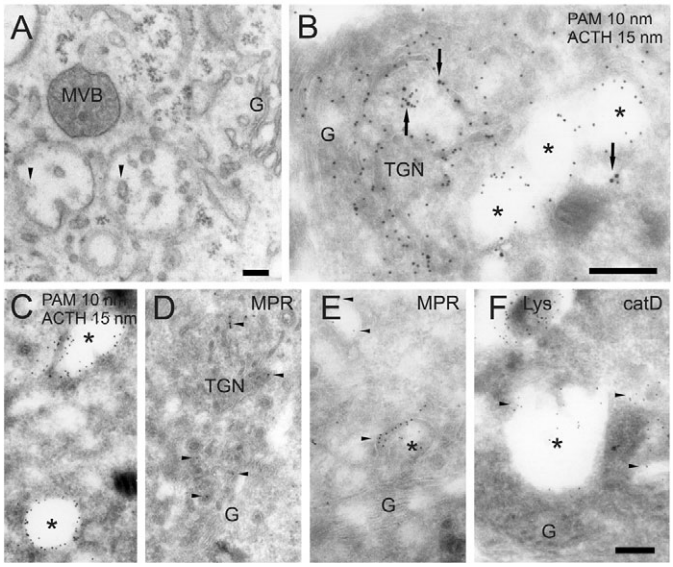

Fig. 5. Trafficking of secretory granule and membrane markers in the formation of mixed organelles. (A) PAM-1 AtT-20 cells were treated with 1 nM ConA for 2 hours. In the TGN area, a normal multivesicular body (MVB) was seen adjacent to vacuoles filled with invaginations and internal vesicles decorated with spike-like electron-dense material (arrowheads). Scale bar: 0.1 μm. Immunoelectron microscopy was used to examine the initial stages of mixed organelle formation in cells treated with 1 nM ConA for 24 hours. PAM (10 nm gold) was observed in vacuoles (asterisks) in the TGN area; little processed ACTH (15 nm gold; arrows) was present (B,C). MPR was present in subdomains of the TGN (D, arrowheads) and in vacuoles in the TGN area (E, asterisk). Cathepsin D accumulated in dilated lysosomes (Lys) and in TGN vacuoles (F, asterisk). Scale bars: 0.25 μm.

After 24 hours of treatment, samples were stained simultaneously with antibody against PAM-1 (10 nm gold) and an antibody that recognizes POMC cleavage products, but not intact POMC (15 nm gold) (Fig. 5B,C). Staining for PAM was prevalent in TGN vacuoles (asterisks), but little processed ACTH (arrows) was present in these vacuoles (Fig. 5B,C). Labeling for mannose 6-phosphate receptor (M6PR; labeled MPR) was present in subdomains of the TGN (Fig. 5D, arrowheads) and in vacuoles near the TGN (Fig. 5E). Accumulation of cathepsin D was also observed in dilated lysosomes and TGN vacuoles (Fig. 5F).

Localization of membrane PAM-1 by immunofluorescence suggested that it might be included in the internal vesicles. To assess this possibility, the localization of PAM, MPR and cathepsin D was examined following treatment with a high dose of ConA (10 nM) for 24 hours. PAM was concentrated in the internal vesicles contained in the mixed organelles (Fig. 6A); the inset in Fig. 6A illustrates the association of PAM with these internal membranes. Staining for PAM was less prevalent on the limiting membranes of the mixed organelles. In control cells, there was little overlap in the distribution of MPR and PAM. Following ConA treatment, MPR, similarly to PAM, accumulated in the internal vesicles of mixed organelles (Fig. 6B) and was also detectable in the vacuoles present around the TGN (Fig. 6B). Cathepsin D was present in both the mixed organelles and in vacuoles in the TGN area (Fig. 6C).

Since immature secretory granules have been well characterized in melanotropes (Back and Soinila, 1996), the POMC-producing cells of the intermediate pituitary, we explored the effect of ConA on this organelle in cultured melanotropes (Fig. 6D-F). Immature secretory granules in melanotropes form near the Golgi and contain small, dense cores (Fig. 6D, arrowheads). In cultured melanotropes treated for 4 hours with 10 nM ConA, vacuoles and enlarged immature granules were apparent (Fig. 6E, asterisks); what appeared to be granule cores were seen in the Golgi stack (Fig. 6E, arrows), suggesting premature condensation. As in AtT-20 cells, mixed organelles were prevalent (Fig. 6F,M). Images suggesting fusion of two mixed organelles (Fig. 6F,M, arrows, right) and fusion of a secretory granule with a mixed organelle (Fig. 6F,M, arrows, left) are shown. One of the mixed organelles (Fig. 6F,M, middle) contained an enlarged electron-dense secretory granule whereas another contained what appeared to be a mitochondrion (Fig. 6F,M).

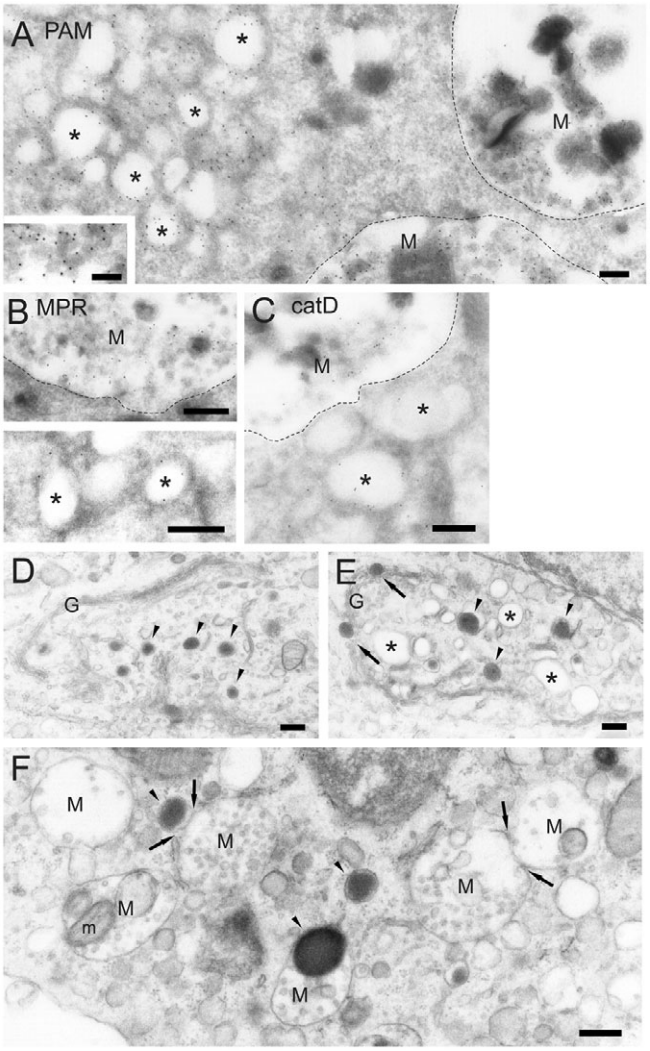

Fig. 6. The internal membranes of mixed organelles. PAM-1 AtT-20 cells were treated with 10 nM ConA for 24 hours before visualization of PAM (A), MPR (B) or cathepsin D (C, catD). PAM was concentrated in the membranes of internal vesicles (inset shows higher magnification), vacuoles in the TGN area (asterisks) and mixed organelles (M). MPR (B) and cathepsin D (C) also accumulated in mixed organelles and were present at lower concentrations in TGN vacuoles. Scale bars: 0.25 μm and 0.1 μm in inset. Primary melanotropes were examined under control conditions (D) or after treatment with 10 nM ConA for 4 hours (E-F). The electron-dense cores of immature secretory granules are indicated with arrowheads. ConA treatment yielded empty vacuoles (asterisk), enlarged immature granules and premature condensation of secretory material in the Golgi stack (E, arrows). Arrows indicate fusion of mixed organelles (M; arrows, right) and a secretory granule (arrowhead) with a mixed organelle (arrows, left) (F). The mixed organelle in the middle contains a large, electron-dense secretory-granule core; the mixed organelle to the left contains a mitochondrion (m). Scale bars: 0.25 μm.

Mixed organelles share features with autophagosomes

The mixed organelles formed in response to ConA treatment clearly include elements of immature secretory granules and lysosomes. Autophagy involves the import of cytoplasmic components into autophagosomes, which then fuse with lysosomes (Klionsky et al., 2008; Marsh et al., 2007; Rubinsztein, 2007). Autophagy begins with formation of a double membrane that sequesters cytoplasm and target organelles, such as mitochondria. Based on electron microscopy, mature mixed organelles do not have double membranes. Since double membranes can be transient, we searched for evidence of their presence as vacuoles first formed in the TGN area and found none. To further compare the formation of mixed organelles to autophagy, we visualized mitochondria in ConA-treated PHM-GFP cells (Fig. 7A) (Weisiger and Fridovich, 1973). Mitochondria remained intact and were mostly excluded from the mixed organelles, which is consistent with the conclusion that macroautophagy is not occurring. The localization of endogenous Atg12 (Hanada et al., 2007), which is covalently bound to Atg5 and targeted at least transiently to autophagosomes (Geng and Klionsky, 2008), was unaltered by treatment with ConA; whether examined after 1 hour or 24 hours of exposure to ConA, Atg12 was present in punctate structures that were distinct from the large mixed organelles (Fig. 7B). Western blot analysis using the same Atg12 antibody revealed a single 53 kDa band in control and ConA-treated cells (data not shown).

LC3/Atg8, a ubiquitin-like protein essential for autophagocytosis, is associated with completed autophagosomes (Geng and Klionsky, 2008; Kabeya et al., 2000; Rubinsztein, 2007). To assess the response of LC3 to ConA, AtT-20 cells transiently expressing LC3-

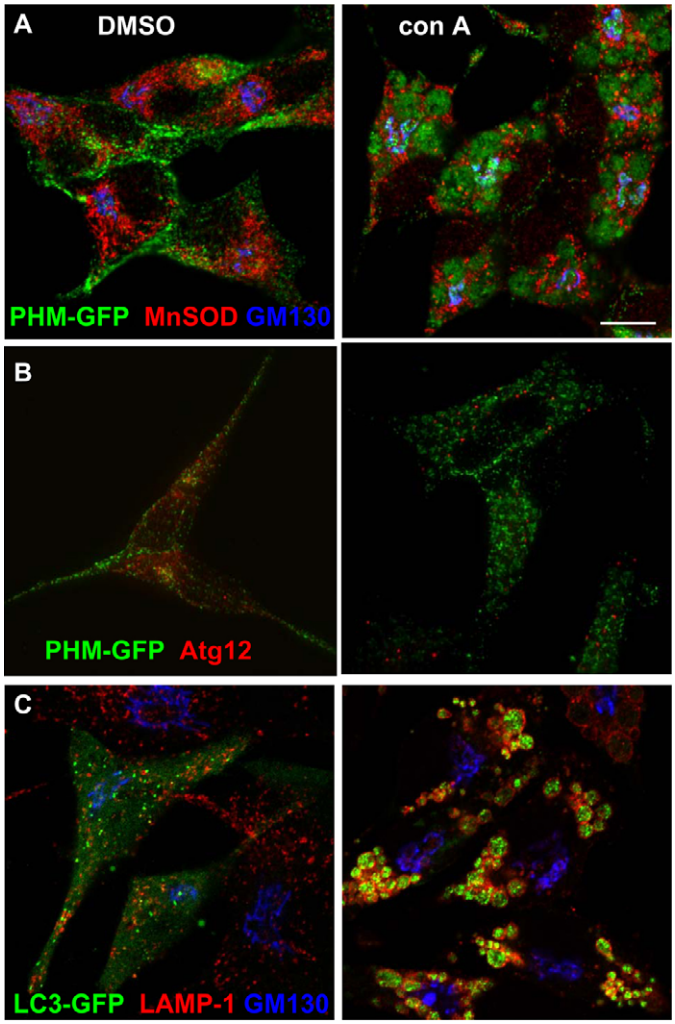

Fig. 7. Mixed organelles are not typical autophagosomes. Localization of the mitochondrial marker MnSOD was evaluated in AtT-20 PHM-GFP cells treated with vehicle (A, left) or 1 nM ConA (A, right). MnSOD was visualized (red) along with PHM-GFP (green) and GM130 (blue). (B) AtT-20 PHM-GFP cells were treated with vehicle or ConA for 8 hours, fixed and visualized after staining for Atg12 (red); deconvolved images. (C) AtT-20 cells were transiently transfected with vector encoding LC3-GFP. 24 hours after the transfection, cells were exposed to DMSO or ConA as in (A). LC3-GFP was visualized (green) with LAMP-1 (red) and GM130 (blue). Scale bar: 10 μm in A,C; 15 μm in B.

GFP were exposed to drug (Fig. 7C). In control cells, LC3-GFP was present throughout the cytosol and was concentrated in puncta distinct from those staining for LAMP-1. Following ConA treatment, most of the LC3-GFP relocated to the interior of the mixed organelles (Fig. 7C); this was in distinct contrast to the behavior of endogenous Atg12, which remained associated with dispersed puncta. Mixed organelles do not have all the accepted properties of autophagosomes, but clearly share some key features, especially following prolonged exposure to ConA.

Protein synthesis is required for ConA-mediated effects on secretory protein localization

If ConA results in the formation of mixed organelles in part by interfering with an early stage in granule maturation, blockade of protein synthesis concurrent with ConA treatment should preclude the formation of mixed organelles. If mixed organelles form solely

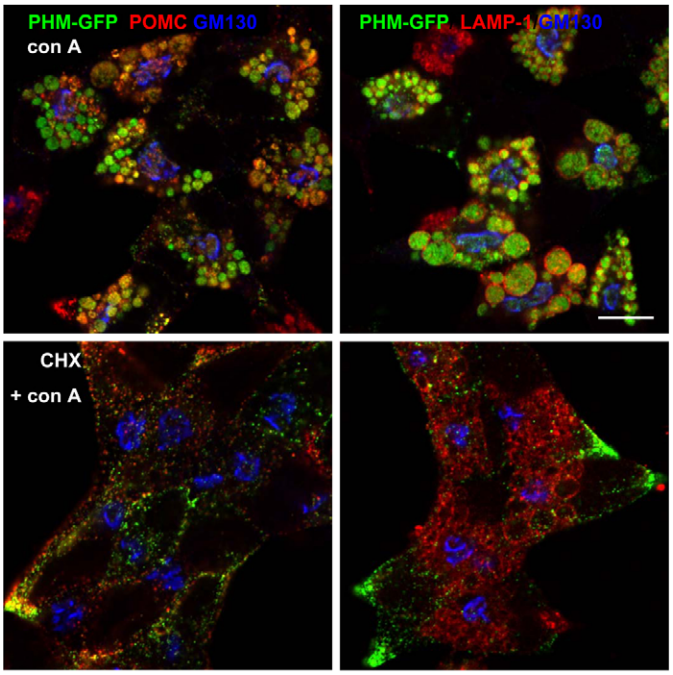

Fig. 8. Requirement of new protein synthesis for ConA-induced collection of secretory proteins into mixed organelles. AtT-20 PHM-GFP cells were subjected to ConA treatment for 24 hours in the absence (top) or presence (bottom) of 10 μM cycloheximide. POMC (left panel, red), LAMP-1 (right panel, red), and GM130 (blue) were visualized along with PHM-GFP (green). Scale bar: 10 μm.

as a result of ConA-induced fusion of mature granules with lysosomes, protein synthesis should not be an essential step in their biogenesis. To distinguish between these possibilities, AtT-20 PHM-GFP cells were treated with ConA in the presence or absence of the protein synthesis inhibitor cycloheximide for 24 hours. As described above, in ConA-treated cells, PHM-GFP and POMC colocalized in the interior of the mixed organelles (Fig. 8, top left) and LAMP-1 staining framed the PHM-GFP-positive mixed organelles (Fig. 8, top right).

As expected, when protein synthesis was inhibited throughout the 24 hours of exposure to ConA, PHM-GFP, POMC and LAMP-1 immunofluorescence diminished in intensity (Fig. 8, bottom). No large PHM-GFP- or POMC-positive mixed organelles were seen (Fig. 8, bottom left). The PHM-GFP and POMC staining that remained was vesicular, comparable to the few mature granules remaining in untreated controls; cycloheximide-treated controls (not shown) were simply depleted of granules (Sobota et al., 2006). Although diminished in intensity, LAMP-1 staining was similar to the pattern seen in the absence of cycloheximide; large vesicular structures were present. In the presence of cycloheximide, the interior of the LAMP-1-positive structures was devoid of soluble secretory-granule proteins (Fig. 8, bottom right). The simplest interpretation of the cycloheximide experiment is that new protein synthesis is required for ConA to exert its effects on soluble secretory protein localization; mature secretory granules located near the plasma membrane were unaffected by ConA treatment.

The fact that LAMP-1 appeared in the outer membranes of the mixed organelles in the absence of new protein synthesis is most plausibly explained by fusion of pre-existing lysosomes with the empty TGN vacuoles that form in the absence of protein synthesis,

as suggested by the ultrastructural (Fig. 4A) and time-lapse (supplementary material Fig. S7) images. Unlike lysosomes, pre-existing peptide-containing secretory granules are excluded from the mixed organelles. Only newly forming peptide-containing granules could be incorporated into mixed organelles.

The role of the V-ATPase protein

If ConA is acting by inhibiting the V-ATPase, shRNA-mediated reductions in V-ATPase levels should have similar effects. Based on studies of the roles of the V_0 and V_1 complexes of the V-ATPase in vacuole fusion and fission in yeast, ConA might be expected to diminish fission, whereas a lack of V_0 might affect fusion (Baars et al., 2007). Since immature granules are short-lived, dynamic structures, whose formation and maturation involve both fusion and fission-mediated remodeling (Kuliawat et al., 1997; Tooze, 1998; Wu et al., 2001), we focused on identifying the earliest effects of reducing V-ATPase levels. In addition to affecting immature secretory-granule formation and function, lack of the V-ATPase would be expected to alter lysosomal function; an essential role for the V-ATPase in cell viability was noted previously (Inoue et al., 1999). A gene expression screen using AtT-20 cDNAs found only background levels of c-subunit mRNA (NM_009729.1), but robust expression of b-subunit mRNA (NM_033617.1; also called c′ and f). Three shRNA constructs directed against V_0b (supplementary material Table S1) were transiently expressed in AtT-20 PAM-1-GFP cells. Based on fluorescence microscopy, expression of each shRNA resulted in dispersion of PAM-1-GFP in the TGN region (Fig. 9A,B). At the electron microscopic level, expression of V_0b-255 shRNA disrupted the normal structure of the TGN (Fig. 9C). In cells expressing V_0b shRNA, empty vacuoles and vacuoles filled with tubular and vesicular structures appeared in the Golgi area (Fig. 9D,E); the internal vesicles and tubules apparent in the shRNA-expressing cells resembled those present in ConA-treated cells. Arrows indicate apposed vacuoles that might be fusing (Fig. 9D). Based on the effects of V-ATPase inhibitors and shRNAs, this complex protein has a key role in the earliest steps of granule formation at the TGN.

Response of SNARE proteins to ConA

To identify biochemical correlates of the morphological response observed, we evaluated the effects of ConA on levels of several SNARE proteins and proteins known to interact with the V-ATPase (Fig. 10). Levels of the endosomal syntaxins syntaxin-7 and syntaxin-13 increased, whereas levels of syntaxin-6, a TGN syntaxin, and SNAP23 and SNAP25, plasma membrane SNARE proteins, were unaltered. Although its cause is not clear, a slight increase in the apparent molecular mass of syntaxin-7 and syntaxin-13 was always observed in ConA-treated cells. Levels of two vesicle SNARE proteins (VAMP2 and VAMP4) were unaltered. Consistent with a deficit in the remodeling of immature granule membranes, levels of γ-adaptin, a subunit of the AP1 complex, were reduced. Levels of βIII-tubulin declined substantially, perhaps contributing to the accumulation of immature granules in the TGN region. Microtubules have an essential role in pH-induced V-ATPase trafficking (Tresguerres et al., 2006) and in glucose-deprivation-induced dissociation of V_0 and V_1 (Xu and Forgac, 2001). Levels of N-cadherin, a plasma membrane cell-cell adhesion molecule, were unaltered.

Discussion

Unlike NH_4Cl and methylamine, macrolide antibiotic V-ATPase inhibitors have a profound effect on soluble and membrane proteins

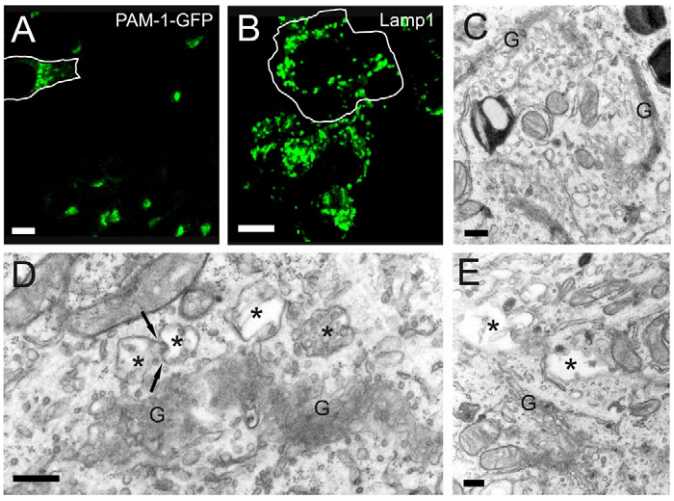

Fig. 9. Silencing of the c-subunit of the V_0 domain of the V-ATPase causes vacuolization of the TGN. shRNA targeting the c-subunit of the V-ATPase was transiently expressed in PAM-1-GFP cells; 48 hours after transfection, cells were fixed and those expressing the shRNA were identified based on DsRed expression. (A,B) Cells expressing the shRNA are outlined; PAM-1 staining was dispersed (A) but lysosomes were not enlarged and LAMP-1 staining was not concentrated near the TGN (B); uptake of DAMP was unaffected. Electron microscopy shows the Golgi area (G) of a nontransfected control cell (C). Vesiculated vacuoles (asterisks) were prevalent in the TGN area of cells expressing the shRNA (D,E); arrows indicate sites at which apposed membranes might be fusing. Scale bars: 10 μm in A,B and 0.25 μm in C-E.

exiting the TGN. In AtT-20 corticotropes, the first effects of these V-ATPase inhibitors include the appearance of TGN vacuoles filled with immature secretory-granule content proteins and swelling of lysosomes. The membranes of the TGN vacuoles invaginate, forming 35-50 nm vesicles that accumulate in the lumen, resembling the internal vesicles characteristic of multivesicular bodies. The TGN vacuoles are often closely apposed to each other and to swollen lysosomes. With time, normal lysosomes disappear and large, mixed organelles that appear to be formed by the fusion of newly formed TGN vacuoles with new and pre-existing lysosomes predominate.

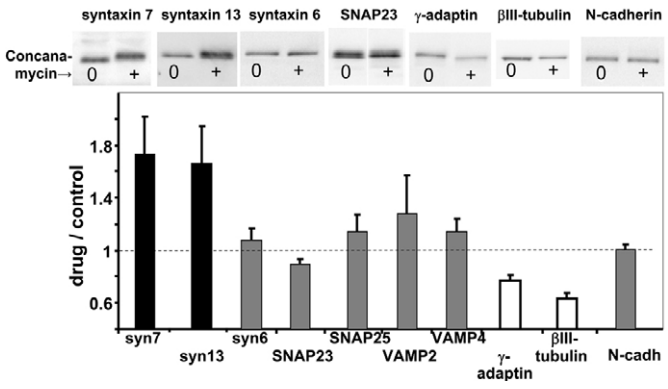

Fig. 10. ConA treatment alters the level of a subset of proteins in AtT-20 cells. AtT-20 PHM-GFP cells treated with ConA (3 nM) or with DMSO vehicle for 8 hours were harvested into SDS lysis buffer for western blot analysis of selected SNARE proteins and other proteins crucial to vesicular trafficking. Signals were quantified using Genegnome and GeneSnap software. Data from repeated analyses of three independent experiments, each with duplicate samples, are pooled, showing mean ± s.e.m. for the ConA/control ratio for each protein. For syntaxin-7, syntaxin-13, γ-adaptin and βIII-tubulin, n=14-18.

By contrast, the cisternae of the Golgi complex remain intact; TGN38 and syntaxin-6 are not included in the mixed organelles. Early endosome markers are also excluded from the mixed organelles. LAMP-1 and VAMP-4 populate the limiting membranes of the mixed organelles. Entry into the internal vesicles is selective, with membrane PAM and mannose-6-phosphate receptor found in internal vesicles.

Lack of a pH gradient does not cause mixed organelle formation

Recent studies in a variety of organisms have demonstrated roles for the macrolide-antibiotic-binding transmembrane V_0 sector of the V-ATPase that are independent of its proton pump activity (Baars et al., 2007; Hiesinger et al., 2005; Lee et al., 2006; Liegeois et al., 2006). Since treatment of AtT-20 cells with NH_4Cl or methylamine neutralized pH gradients but did not generate mixed organelles, their formation is not simply dependent on lack of a pH gradient. Transient knockdown of the lipoprotein component of V_0 altered secretory-granule formation in a similar manner. Selective and verifiable silencing of V_0 and V_1 will be required to distinguish pump-dependent and pump-independent actions of the V-ATPase. Our electron micrographs and live-cell imaging experiments suggest that prolonged ConA treatment causes immature granules to fuse with lysosomes, forming mixed organelles. The occurrence of fusion is consistent with the observed dose- and time-dependent increase in mixed organelle size. Homotypic fusion of immature secretory granules is an established part of secretory-granule biogenesis in lactotropes and PC12 cells (Cochilla et al., 2000; Wendler et al., 2001). In response to the sudden removal of secretory stimuli, prolactin and thyroid-stimulating hormone containing secretory granules fuse with lysosomes in the process of crinophagy (Farquhar, 1977; Noda and Farquhar, 1992).

The question is why fusion occurs after prolonged ConA treatment. The formation of immature granules normally involves vesicle fusion, whereas maturation involves fission-mediated remodeling (Kuliawat et al., 1997; Tooze, 1998; Wu et al., 2001). An inability to remodel membranes may leave the immature granules fusion competent, indirectly allowing fusion to occur. Although it is clear that V-ATPase subunits have an important role in many membrane fusion events, the underlying mechanisms are poorly understood (Kontani et al., 2005; Lee et al., 2006; Mohler et al., 2002). In yeast, pump-independent fusion of smaller vacuoles into large vacuoles occurs with just V_0 whereas ConA blocks V_1-mediated vacuolar fission (Baars et al., 2007). *C. elegans* with VHA-5 (V_0a1) mutations accumulate multivesicular bodies that are unable to fuse with the plasma membrane (Liegeois et al., 2006). The large multivesicular bodies observed in these *C. elegans* mutants resemble the mixed organelles formed in AtT-20 cells as a result of ConA treatment. In vitro studies will be required to distinguish the initial effects from the later consequences.

Secretion and the V-ATPase

Our studies show that stimulated secretion of the soluble components of secretory granules is blocked by ConA treatment. Immature secretory granules fail to mature, and secretory products accumulate in the mixed organelles that remain near the TGN. The lack of stimulated secretion could reflect an inability to remove key components of the immature secretory-granule membrane in the presence of ConA or failure to translocate granules to the plasma membrane. For example, removal of VAMP4 and synaptotagmin IV is crucial for granule maturation and acquisition of regulatory competence (Eaton et al., 2000), and VAMP4 accumulates in the limiting membrane of the mixed organelles that form in ConA-treated cells. The mechanism by which the V_0a1 subunit affects synaptic vesicle exocytosis in *Drosophila* is distinctly different (Hiesinger et al., 2005). Interaction of V_0a1 with tSNAREs might guide V_0 into vesicle and acceptor membranes to allow formation of a fusion pore; this function of V_0 is likely to be independent of V_1, whose presence would inhibit membrane apposition (Hiesinger et al., 2005).

In mouse proximal tubule cells, budding and formation of endosome-derived carrier vesicles has been linked to the V-ATPase; Arf6 interacts with V_0c, and ARNO interacts with V_0a2, (Hurtado-Lorenzo et al., 2006). These interactions are dependent on luminal acidification; V-ATPase inhibitors perturb recruitment and scaffolding of Arf6 and ARNO to endosomal membranes, hindering early to late endosome trafficking (Hurtado-Lorenzo et al., 2006). ConA might block the maturation of immature granules in a similar manner, mediating membrane budding and acting as a component of the molecular machinery that senses luminal pH.

Why do mixed organelles appear in this paradigm?

BafA1 and ConA are frequently used for shorter times at higher concentrations. The long treatment time used here was based on earlier studies of PC12 cells (Taupenot et al., 2005). Although granule maturation is blocked, mature granules are not dramatically affected. The mixed organelles appear only as newly synthesized secretory-granule and lysosomal content proteins accumulate; if disrupting granule maturation with ConA is the key event, accumulation of enough newly synthesized granule and lysosomal protein to form mixed organelles would be expected to require time. With the electron microscope, it is clear that TGN vacuoles and enlarged lysosomes are detectable within 4 hours. Mixed organelles form as the result of a biosynthetic process gone awry, not as a result of fusion of mature secretory granules. Our results are consistent with other studies that have evaluated the morphology of secretory pathway compartments in response to V-ATPase inhibitors. Electron microscopic analysis of *Xenopus* intermediate pituitary cells treated with BafA1 demonstrated the appearance of vacuolar structures adjacent to the TGN, along with a dramatic decrease in the number of secretory granules (Schoonderwoert et al., 2000); because treatment times were short, formation of mixed organelles was not observed in this study.

The V-ATPase inhibitors seem to be acting at membrane-budding steps where the produced small organelle will have an internal pH below the cytosolic pH. Removal of VAMP4, which is an essential step in granule maturation, could be blocked. Continued protein synthesis would result in continued production of immature granules. If the ability of immature granules to undergo homotypic fusion is not blocked, fusion to immature granules and lysosomes might continue, yielding large mixed organelles.

For ACTH-producing cells, as for insulin-producing cells (Marsh et al., 2007), degradation of product hormones is not normally seen; virtually all the POMC produced in a pulse labeling is recovered as mature stored or secreted peptides (Mains and Eipper, 1981). However, in the face of reduced demand for secretory product, lactotropes and β-cells eliminate mature granules through the process of crinophagy (Farquhar, 1977; Marsh et al., 2007). In this normal response to diminished demand, secretory granules fuse with lysosomes. The granule fusion process initiated by ConA might mimic the process normally used during crinophagy.

The maturation process initiated in immature granules involves proteolytic processing of prohormones, concentration of soluble

content and remodeling of granule membranes. Newly synthesized lysosomal enzymes that enter the regulated secretory pathway are removed along with their mannose-6-phosphate receptors (Kuliawat et al., 1997). Lysosomal membrane proteins such as LAMP-1 might reach late endosomes and lysosomes directly from the TGN (Peters and von Figura, 1994). The internal vesicles that accumulate following ConA treatment contain PAM and mannose-6-phosphate receptor, which are normally retrieved from immature granules, but lack LAMP-1 and VAMP-4. Failure to remove VAMP4 would be expected to contribute to a blockade of regulated secretion.

A previous study did not detect mixed organelles following prolonged treatment of PC12 cells with nanomolar concentrations of BafA1 (Taupenot et al., 2005), and our results with PC-12 cells confirm this. Since we see formation of mixed organelles in fibroblasts and in two neuroendocrine lines, it is plausible that particular protein components of the V-ATPase in the PC-12 cells are distinct from those in AtT-20, GH3 and 3T3 cells. A biochemical comparison of the four cell lines will be needed to resolve these questions. Studies of *C. elegans*, *Drosophila* and mammalian tissues support the generality of our results.

Are the mixed organelles autophagosomes?

Cellular constituents can be degraded and recycled through the process of autophagy. Inclusion of lysosomes in the mixed organelles prompted us to compare the mixed organelles to autophagosomes. LC-3, the mammalian orthologue of yeast Atg8, is a cytosolic protein that assembles on autophagosomes as they form, undergoing a series of processing steps that allow it to enter their interior. Although LC3-GFP was present, the mixed organelles do not have other features of autophagosomes. First, mitochondria are excluded from the mixed organelles. Second, even at early times, no phagophore membrane is apparent (Marsh et al., 2007). Third, Atg12, an essential component of autophagosomes, is not associated with the mixed organelles. Fourth, upon removal of V-ATPase inhibitor, cells slowly rid themselves of these mixed organelles and recover; staining for soluble content proteins in the mixed organelles disappears, presumably as a result of proteolysis, and the normal complement of secretory granules and lysosomes reappears. Whether LC3-GFP recognizes and enters the mixed organelles in a manner similar to that used to enter autophagosomes is not yet clear.

The mixed organelles in AtT-20 cells differ from autophagosomes because they are filled with uniformly sized vesicles containing secretory pathway proteins instead of cytoplasmic fragments or organelles. Formation of multivesicular bodies in the TGN is not a feature associated with autophagy. This process has been described during crinophagy; the destruction of secretory granules when secretion is suppressed. In prolactin cells undergoing crinophagy, mature secretory granules and excessive endoplasmic reticulum are incorporated into autophagic structures whereas immature secretory granules are incorporated into multivesicular bodies (Smith and Farquhar, 1966). In both AtT-20 cells and pituitary melanotropes, ConA induces the formation of multivesicular bodies in the TGN. In AtT-20 cells, the multivesicular bodies fuse with lysosomes to form multivesiculated mixed organelles that contain autophagic debris in melanotropes when mature.

Materials and Methods

Antibodies

The following rabbit antisera were used for immunocytochemistry: POMC/ACTH (JH93, 1:1000) directed against the N-terminal of ACTH (Zhou et al., 1993), TGN38 (JH1481, 1:1000) and VAMP4 (Synaptic Systems, 1:500). Monoclonal antibodies against GM130 (1:500), syntaxin-6 (1:250, Covance), procathepsin B (1:1000, gift from Peter Arvan, University of Michigan, Ann Arbor, MI), LAMP-1 (1:50, Developmental Studies Hybridoma Bank), Atg12 (Cell Signaling Technology, Inc., 1:1000) and manganese superoxide dismutase (1:500, Upstate) were sourced. For immunoblot analyses, rabbit polyclonal antisera against PC1 (JH888, 1:1000) (Zhou and Mains, 1994), γMSH (JH189, 1:1000) (Cullen and Mains, 1987), PHM (JH1761, 1:1000) (El Meskini et al., 2001), syntaxin-13 (Abcam), syntaxin-7 (Synaptic Systems), pan-cadherin (Sigma) and SNAP23 (Abcam) and monoclonal antibodies against VAMP2 (Synaptic Systems), syntaxin-6 (BDTL), SNAP25 (BDTL), βIII tubulin (Covance), α-, β- and γ-adaptin (BDTL), N-cadherin (BDTL) and Atg12 (Cell Signaling Technology) were used. For electron microscopic immunohistochemistry, the following rabbit antisera were used: exon A (JH629, 1:200) directed against PAM-1(409-497), ACTH (Kathy, 1:1000) directed against ACTH(25-39), cation-independent 300 kDa mannose-6-phosphate receptor (I-5, 1:100) and cathepsin D (SII-10, 1:50). The MPR and cathepsin D antibodies were gifts from Stefan Höning (University of Cologne, Cologne, Germany).

Cell culture and drug treatment paradigms

PAM-2-GFP was constructed in pEGFP-N2 (Clontech) by fusing in-frame the C-terminus of PAM (...PAPSS976) at an engineered *Sma*I site, incorporating the short intervening linker derived from pEGFP-N2 (PGIHRPVAT), followed by the N-terminus of EGFP (M1VSKG...). AtT-20 cells stably expressing PAM-1 (Milgram et al., 1992), PAM-1-GFP (J.A.S., B.A.E. and R.E.M., unpublished), PHM fused to green fluorescent protein (PHM-GFP) and PHM fused to the pH-sensitive pHluorin (PHM-pHluorin) (Miesenbock et al., 1998) were maintained in culture as described (Sobota et al., 2006). Short hairpin RNAs (shRNAs) directed against several of the V-ATPase subunits were constructed in the RNAi-Ready-pSiren-DNRDsRed-Express vector (Clontech), which places shRNA expression under control of the human U6 promoter and DsRed expression under control of the CMV promoter. Sequences for shRNAs were selected using the rules at http://bioinfo.clontech.com/rnaidesigner/frontpage.jsp and http://imgenex.com/sirna_tool_details.php?opt=view_result (supplementary material Table S1). All constructs were verified by DNA sequencing. The LC3-GFP plasmid was a gift from Tamotsu Yoshimori (Osaka University, Osaka, Japan) (Kabeya et al., 2000).

Cells were incubated with all alkalinizing drugs for 22-24 hours. Concanamycin A and bafilomycin A1 (Sigma) were used at concentrations of 1 nM and 20 nM, respectively. Ammonium chloride (Sigma) was used at 2.5 mM; methylamine (Sigma) was used at 5 mM. Alkalinization was assessed in drug-treated live cells using acridine orange (Sobota et al., 2006) or 3-(2,4-dinitroanilino)-3′-amino-N-methyldipropylamine (DAMP). After a 30 minute incubation followed by fixation, DAMP was visualized using antibody to DNP (Anderson et al., 1984). In addition, AtT-20 cells stably expressing PHM-pHluorin and placed into medium lacking phenol red were photographed live after different times of exposure to concanamycin A; untreated cells were fixed, permeabilized and equilibrated with buffers titrated to pH 5.0, 5.5, 6.0, 6.5, 6.75, 7.0, 7.25 and 7.5 to generate a standard curve relating fluorescence intensity to pH. To assess the role of protein synthesis on the effects of ConA, 10 μM cycloheximide was added to the incubation medium. All drugs were prepared at their final concentrations in complete serum-free medium (CSFM) containing ITS (DMEM-F12 supplemented with 100 U/ml penicillin, 100 μg/ml streptomycin, insulin-transferrin-selenium from Invitrogen or Mediatech and 1 mg/ml fatty acid-free bovine serum albumin).

For primary cultures of melanotropes, adult male Sprague-Dawley rats (Scanbur, Sollentuna, Sweden) were decapitated under carbon dioxide anesthesia. The neurointermediate lobe was separated from the anterior pituitary and intermediate lobe fragments were dissociated with collagenase (Sigma, type II, 4 mg/ml), hyaluronidase (Sigma, type IV, 1 mg/ml) and DNase (Sigma, type I, 0.01 mg/ml) for 20 minutes followed by trypsin (Sigma, 2.5 mg/ml) for 15 minutes, then plated in poly-L-lysine-treated dishes and cultured for 3 days before treatment (May et al., 1989).

Secretion experiments and enzyme assays

AtT-20 PHM-GFP cells were plated in duplicate wells on poly-L-lysine-coated plastic dishes and maintained in culture for 2 days (Sobota et al., 2006). To determine basal secretion over a 24 hour period, cells were initially rinsed in CSFM (0.1 mg/ml BSA), replaced with CSFM containing DMSO vehicle, ConA or ammonium chloride, and media and cells were harvested 24 hours later. Medium was centrifuged to remove non-adherent cells and protease inhibitors were added. Cells were harvested in 20 mM Na-*N*-Tris[hydroxymethyl]methyl-2-aminoethanesulfonic acid (TES), 10 mM mannitol, 1% Triton X-100, pH 7.4 (TMT) with PMSF and protease inhibitors (Sobota et al., 2006). TMT extracts were frozen and thawed three times and centrifuged to remove debris. For assessment of regulated secretion, cells were plated and pretreated with drug as described above. Before media collection, cells were initially rinsed for three 30 minute periods with CSFM containing vehicle or drug, followed by collection of 30 minute basal medium and 30 minute stimulation with 2 mM $BaCl_2$. Secretion over 24 hours was assessed by western blot analysis; equal volumes of medium and cell extracts were fractionated by SDS-PAGE, transferred to PVDF and probed with antibodies against PC1, γMSH or PHM. Signals in the linear range were quantified using GeneTools software (Syngene). Medium samples and cell extracts from 30 minute basal and stimulation collections were assayed for PHM activity using ^{125}I

labeled α-*N*-acetyl-Tyr-Val-Gly as substrate (Kolhekar et al., 1997). Samples were assayed in duplicate and reactions were carried out for 1 hour.

Immunofluorescence and confocal microscopy

Cells were plated onto poly-L-lysine-coated 0.17 mm glass coverslips (Fisher Scientific) and maintained in DMEM-F12 for 2 days. Following drug treatment, cells were fixed in prewarmed 4% formaldehyde in PBS for 30 minutes at room temperature, processed for immunocytochemistry and visualized by confocal microscopy (Sobota et al., 2006). For live-cell imaging with a Leica TCS SP2 confocal microscope, cells were incubated in DMEM-HEPES with 1 mg/ml bovine serum albumin at 37°C.

Electron microscopy and immunoelectron microscopy

For electron microscopy, cells were fixed with 2.5% glutaraldehyde in 0.1 M cacodylate buffer for 30 minutes, postfixed with 1% osmium tetroxide and 1% potassium ferrocyanide for 30 minutes, dehydrated and embedded in Epon. Sections were poststained with lead citrate and uranyl acetate and viewed with a Jeol 1200 EX II electron microscope. For cryosectioning and immunogold labelling, the cells were fixed with 4% paraformaldehyde in 2% sucrose, 0.1 M phosphate buffer for 2 hours, scraped and centrifuged in gelatin. Immunolabeling was performed as described earlier (Sobota et al., 2006), and acidic organelles were visualized ultrastructurally using the DAMP method (Anderson et al., 1984).

Transferrin and dextran uptake

AtT-20 PAM-1 cells were pretreated with vehicle or ConA for 24 hours as described. Cells were rinsed twice with serum-free medium lacking transferrin 30 minutes before the experiment, followed by incubation with medium containing 0.1 mg/ml transferrin conjugated to Alexa Fluor 488 (Invitrogen) for 10 minutes. Following a brief rinse, cells were fixed and processed for immunocytochemistry as described above. To label lysosomes, AtT-20 PHM-GFP cells were incubated with TRITC-dextran for 1 hour followed by an overnight chase, addition of ConA and live-cell imaging.

Supported by National Institutes of Health grants DK-32948, DE-017094 and DE-007302; the Perklén Foundation and the Liv och Hälsa Foundation. We thank the Electron Microscopy Unit of the Institute of Biotechnology, University of Helsinki for providing laboratory facilities. Deposited in PMC for release after 12 months.

References

Anderson, R. G., Falck, J. R., Goldstein, J. L. and Brown, M. S. (1984). Visualization of acidic organelles in intact cells by electron microscopy. *Proc. Natl. Acad. Sci. USA* **81**, 4838-4842.

Baars, T. L., Petri, S., Peters, C. and Mayer, A. (2007). Role of the V-ATPase in regulation of the vacuolar fission-fusion equilibrium. *Mol. Biol. Cell* **18**, 3873-3882.

Back, N. and Soinila, S. (1996). Dose-dependent effects of chloroquine on secretory granule formation in the melanotroph. *Acta Anat.* **156**, 307-314.

Bayer, M. J., Reese, C., Buhler, S., Peters, C. and Mayer, A. (2003). Vacuole membrane fusion: V0 functions after trans-SNARE pairing and is coupled to the Ca^{2+}-releasing channel. *J. Cell Biol.* **162**, 211-222.

Beyenbach, K. W. and Wieczorek, H. (2006). The V-type H^+ ATPase: molecular structure and function, physiological roles and regulation. *J. Exp. Biol.* **209**, 577-589.

Bowman, B. J. and Bowman, E. J. (2002). Mutations in subunit C of the vacuolar ATPase confer resistance to bafilomycin and identify a conserved antibiotic binding site. *J. Biol. Chem.* **277**, 3965-3972.

Bowman, E. J., Siebers, A. and Altendorf, K. (1988). Bafilomycins: a class of inhibitors of membrane ATPases from microorganisms, animal cells, and plant cells. *Proc. Natl. Acad. Sci. USA* **85**, 7972-7976.

Chernyshev, A. V., Tarasov, P. A., Semianov, K. A., Nekrasov, V. M., Hoekstra, A. G. and Maltsev, P. (2008). Erythrocyte lysis in isotonic solution of ammonium chloride: Theoretical modelling and experimental verification. *J. Theoret. Biol.* **251**, 93-107.

Cochilla, A. J., Angleson, J. K. and Betz, W. J. (2000). Differential regulation of granule-to-granule and granule-to-plasma membrane fusion during secretion from rat pituitary lactotrophs. *J. Cell Biol.* **150**, 839-848.

Colomer, V., Kicska, G. A. and Rindler, M. J. (1996). Secretory granule content proteins and the luminal domains of granule membrane proteins aggregate in vitro at mildly acidic pH. *J. Biol. Chem.* **271**, 48-55.

Cullen, E. I. and Mains, R. E. (1987). Biosynthesis of amidated joining peptide from pro-adrenocorticotropin-endorphin. *Mol. Endocrinol.* **1**, 583-594.

Drose, S., Bindseil, K. U., Bowman, E. J., Siebers, A., Zeeck, A. and Altendorf, K. (1993). Inhibitory effect of modified bafilomycins and concanamycins on P- and V-type adenosinetriphosphatases. *Biochemistry* **32**, 3902-3906.

Eaton, B. A., Haugwitz, M., Lau, D. and Moore, H. P. (2000). Biogenesis of regulated exocytotic carriers in neuroendocrine cells. *J. Neurosci.* **20**, 7334-7344.

El Meskini, R., Galano, G. J., Marx, R., Mains, R. E. and Eipper, B. A. (2001). Targeting of membrane proteins to the regulated secretory pathway in anterior pituitary endocrine cells. *J. Biol. Chem.* **276**, 3384-3393.

Farquhar, M. G. (1977). Secretion and crinophagy in prolactin cells. *Adv. Exp. Med. Biol.* **80**, 37-94.

Forgac, M. (1999). Structure and properties of the vacuolar (H+)-ATPases. *J. Biol. Chem.* **274**, 12951-12954.

Forgac, M. (2007). Vacuolar ATPases: rotary proton pumps in physiology and pathophysiology. *Nat. Rev. Mol. Cell Biol.* **8**, 917-929.

Geng, J. and Klionsky, D. J. (2008). The Atg8 and Atg12 ubiquitin-like conjugation systems in macroautophagy. 'Protein modifications: beyond the usual suspects' review series. *EMBO Rep.* **9**, 859-864.

Hanada, T., Noda, N. N., Satomi, Y., Ichimura, Y., Fujioka, Y. and Ohsumi, Y. (2007). The Atg12-Atg5 conjugate has a novel E3-like activity for protein lipidation in autophagy. *J. Biol. Chem.* **282**, 37298-37302.

Hediger, M. A., Romero, M. F., Peng, J. B., Rolfs, A., Takanaga, H. and Bruford, E. A. (2004). The ABCs of solute carriers: physiological, pathological and therapeutic implications of human membrane transport proteinsIntroduction. *Pflugers Arch.* **447**, 465-468.

Hiesinger, P. R., Fayyazuddin, A., Mehta, S. Q., Rosenmund, T., Schulze, K. L., Zhai, R. G., Verstreken, P., Cao, Y., Zhou, Y., Kunz, J. et al. (2005). The v-ATPase V0 subunit a1 is required for a late step in synaptic vesicle exocytosis in Drosophila. *Cell* **121**, 607-620.

Hurtado-Lorenzo, A., Skinner, M., El Annan, J., Futai, M., Sun-Wada, G. H., Bourgoin, S., Casanova, J., Wildeman, A., Bechoua, S., Ausiello, D. A. et al. (2006). V-ATPase interacts with ARNO and Arf6 in early endosomes and regulates the protein degradative pathway. *Nat. Cell Biol.* **8**, 124-136.

Huss, M., Ingenhorst, G., Konig, S., Gassel, M., Drose, S., Zeeck, A., Altendorf, K. and Wieczorek, H. (2002). Concanamycin A, the specific inhibitor of V-ATPases, binds to the V(o) subunit c. *J. Biol. Chem.* **277**, 40544-40548.

Inoue, H., Noumi, T., Nagata, M., Murakami, H. and Kanazawa, H. (1999). Targeted disruption of the gene encoding the proteolipid subunit of mouse vacuolar H(+)-ATPase leads to early embryonic lethality. *Biochim. Biophys. Acta* **1413**, 130-138.

Kabeya, Y., Mizushima, N., Ueno, T., Yamamoto, A., Kirisako, T., Noda, T., Kominami, E., Ohsumi, Y. and Yoshimori, T. (2000). LC3, a mammalian homologue of yeast Apg8p, is localized in autophagosome membranes after processing. *EMBO J.* **19**, 5720-5728.

Klionsky, D. J., Abeliovich, H., Agostinis, P., Agrawal, D. K., Aliev, G., Askew, D. S., Baba, M., Baehrecke, E. H., Bahr, B. A., Ballabio, A. et al. (2008). Guidelines for the use and interpretation of assays for monitoring autophagy in higher eukaryotes. *Autophagy* **4**, 151-175.

Kolhekar, A. S., Keutmann, H. T., Mains, R. E., Quon, A. S. and Eipper, B. A. (1997). Peptidylglycine alpha-hydroxylating monooxygenase: active site residues, disulfide linkages, and a two-domain model of the catalytic core. *Biochemistry* **36**, 10901-10909.

Kontani, K., Moskowitz, I. P. and Rothman, J. H. (2005). Repression of cell-cell fusion by components of the C. elegans vacuolar ATPase complex. *Dev. Cell* **8**, 787-794.

Kuliawat, R., Klumperman, J., Ludwig, T. and Arvan, P. (1997). Differential sorting of lysosomal enzymes out of the regulated secretory pathway in pancreatic beta-cells. *J. Cell Biol.* **137**, 595-608.

Lee, S. H., Rho, J., Jeong, D., Sul, J. Y., Kim, T., Kim, N., Kang, J. S., Miyamoto, T., Suda, T., Lee, S. K. et al. (2006). v-ATPase V0 subunit d2-deficient mice exhibit impaired osteoclast fusion and increased bone formation. *Nat. Med.* **12**, 1403-1409.

Liegeois, S., Benedetto, A., Garnier, J. M., Schwab, Y. and Labouesse, M. (2006). The V0-ATPase mediates apical secretion of exosomes containing Hedgehog-related proteins in Caenorhabditis elegans. *J. Cell Biol.* **173**, 949-961.

Ma, X. M., Wang, Y., Ferraro, F., Mains, R. E. and Eipper, B. A. (2008). Kalirin-7 is an essential component of both shaft and spine excitatory synapses in hippocampal interneurons. *J. Neurosci.* **28**, 711-724.

Madsen, E. C. and Gitlin, J. D. (2008). Zebrafish mutants calamity and catastrophe define critical pathways of gene-nutrient interactions in developmental copper metabolism. *PLOS Genetics* **4**, e1000261.

Mains, R. E. and Eipper, B. A. (1981). Coordinate, equimolar secretion of smaller peptide products derived from pro-ACTH/endorphin by mouse pituitary tumor cells. *J. Cell Biol.* **89**, 21-28.

Mains, R. E. and May, V. (1988). The role of a low pH intracellular compartment in the processing, storage, and secretion of ACTH and endorphin. *J. Biol. Chem.* **263**, 7887-7894.

Marsh, B. J., Soden, C., Alarcon, C., Wicksteed, B. L., Yaekura, K. and Rhodes, C. J. (2007). Regulated autophagy controls hormone content in secretory-deficient pancreatic endocrine beta-cells. *Mol. Endocrinol.* **21**, 2255-2269.

Marshansky, V. and Futai, M. (2008). The V-type H+-ATPase in vesicular trafficking: targeting, regulation and function. *Curr. Opin. Cell Biol.* **20**, 415-426.

May, V., Stoffers, D. A. and Eipper, B. A. (1989). Proadrenocorticotropin/endorphin production and messenger ribonucleic acid levels in primary intermediate pituitary cultures: effects of serum, isoproterenol, and dibutyryl adenosine 3′,5′-monophosphate. *Endocrinology* **124**, 157-166.

Miesenbock, G., De Angelis, D. A. and Rothman, J. E. (1998). Visualizing secretion and synaptic transmission with pH-sensitive green fluorescent proteins. *Nature* **394**, 192-195.

Milgram, S. L., Johnson, R. C. and Mains, R. E. (1992). Expression of individual forms of peptidylglycine alpha-amidating monooxygenase in AtT-20 cells: endoproteolytic processing and routing to secretory granules. *J. Cell Biol.* **117**, 717-728.

Mohler, W. A., Shemer, G., del Campo, J. J., Valansi, C., Opoku-Serebuoh, E., Scranton, V., Assaf, N., White, J. G. and Podbilewicz, B. (2002). The type I membrane protein EFF-1 is essential for developmental cell fusion. *Dev. Cell* **2**, 355-362.

Morel, N. (2003). Neurotransmitter release: the dark side of the vacuolar-H+ATPase. *Biol. Cell* **95**, 453-457.
Morel, N., Dedieu, J. C. and Philippe, J. M. (2003). Specific sorting of the a1 isoform of the V-H+ATPase a subunit to nerve terminals where it associates with both synaptic vesicles and the presynaptic plasma membrane. *J. Cell Sci.* **116**, 4751-4762.
Nishi, T. and Forgac, M. (2002). The vacuolar (H+)-ATPases-nature's most versatile proton pumps. *Nat. Rev. Mol. Cell Biol.* **3**, 94-103.
Noda, T. and Farquhar, M. G. (1992). A non-autophagic pathway for diversion of ER secretory proteins to lysosomes. *J. Cell Biol.* **119**, 85-97.
Parsons, S. M. (2000). Transport mechanisms in acetylcholine and monoamine storage. *FASEB J.* **14**, 2423-2434.
Peters, C. and von Figura, K. (1994). Biogenesis of lysosomal membranes. *FEBS Lett.* **346**, 108-114.
Peters, C., Bayer, M. J., Buhler, S., Andersen, J. S., Mann, M. and Mayer, A. (2001). Trans-complex formation by proteolipid channels in the terminal phase of membrane fusion. *Nature* **409**, 581-588.
Rubinsztein, D. C. (2007). Autophagy induction rescues toxicity mediated by proteasome inhibition. *Neuron* **54**, 854-856.
Schmidt, W. K. and Moore, H. P. (1995). Ionic milieu controls the compartment-specific activation of pro-opiomelanocortin processing in AtT-20 cells. *Mol. Biol. Cell* **6**, 1271-1285.
Schnabel, E., Mains, R. E. and Farquhar, M. G. (1989). Proteolytic processing of pro-ACTH/endorphin begins in the Golgi complex of pituitary corticotropes and AtT-20 cells. *Mol. Endocrinol.* **3**, 1223-1235.
Schoonderwoert, V. T. and Martens, G. J. (2001). Proton pumping in the secretory pathway. *J. Membr. Biol.* **182**, 159-169.
Schoonderwoert, V. T., Holthuis, J. C., Tanaka, S., Tooze, S. A. and Martens, G. J. (2000). Inhibition of the vacuolar H+-ATPase perturbs the transport, sorting, processing and release of regulated secretory proteins. *Eur. J. Biochem.* **267**, 5646-5654.
Seidah, N. G. and Prat, A. (2002). Precursor convertases in the secretory pathway, cytosol and extracellular milieu. *Essays Biochem.* **38**, 79-94.
Seidah, N. G., Day, R. and Chretien, M. (1993). The family of pro-hormone and pro-protein convertases. *Biochem. Soc. Trans.* **21**, 685-691.
Smith, R. E. and Farquhar, M. G. (1966). Lysosome function in the regulation of the secretory process in cells of the anterior pituitary gland. *J. Cell Biol.* **31**, 319-347.
Sobota, J. A., Ferraro, F., Back, N., Eipper, B. A. and Mains, R. E. (2006). Not all secretory granules are created equal: partitioning of soluble content proteins. *Mol. Biol. Cell* **17**, 5038-5052.
Stevens, T. H. and Forgac, M. (1997). Structure, function and regulation of the vacuolar (H+)-ATPase. *Annu. Rev. Cell Dev. Biol.* **13**, 779-808.
Sun-Wada, G. H., Toyomura, T., Murata, Y., Yamamoto, A., Futai, M. and Wada, Y. (2006). The a3 isoform of V-ATPase regulates insulin secretion from pancreatic beta-cells. *J. Cell Sci.* **119**, 4531-4540.
Taupenot, L., Harper, K. L. and O'Connor, D. T. (2005). Role of H+-ATPase-mediated acidification in sorting and release of the regulated secretory protein chromogranin A: evidence for a vesiculogenic function. *J. Biol. Chem.* **280**, 3885-3897.
Tooze, S. A. (1998). Biogenesis of secretory granules in the trans-Golgi network of neuroendocrine and endocrine cells. *Biochim. Biophys. Acta* **1404**, 231-244.
Tresguerres, M., Parks, S. K., Fatoh, F. and Goss, G. G. (2006). Microtubule-dependent relocation of brancial V-H+-ATPase to the basolateral membrane of the Pacific spiny dogfish (Squalus acanthias): a role in base secretion. *J. Exp. Biol.* **209**, 599-609.
Wang, Y., Inoue, T. and Forgac, M. (2005). Subunit a of the yeast V-ATPase participates in binding of bafilomycin. *J. Biol. Chem.* **280**, 40481-40488.
Weimer, R. M. and Jorgensen, E. M. (2003). Controversies in synaptic vesicle exocytosis. *J. Cell Sci.* **116**, 3661-3666.
Weisiger, R. A. and Fridovich, I. (1973). Superoxide dismutase: organelle specificity. *J. Biol. Chem.* **248**, 3582-3592.
Wendler, F., Page, L., Urbe, S. and Tooze, S. A. (2001). Homotypic fusion of immature secretory granules during maturation requires syntaxin 6. *Mol. Biol. Cell* **12**, 1699-1709.
Wu, M. M., Grabe, M., Adams, S., Tsien, R. Y., Moore, H. P. and Machen, T. E. (2001). Mechanisms of pH regulation in the regulated secretory pathway. *J. Biol. Chem.* **276**, 33027-33035.
Xu, T. and Forgac, M. (2001). Microtubules are involved in glucose-dependent dissociation of the yeast vacuolar [H+]-ATPase in vivo. *J. Biol. Chem.* **276**, 24855-24861.
Zhou, A. and Mains, R. E. (1994). Endoproteolytic processing of proopiomelanocortin and prohormone convertases 1 and 2 in neuroendocrine cells overexpressing prohormone convertases 1 or 2. *J. Biol. Chem.* **269**, 17440-17447.
Zhou, A., Bloomquist, B. T. and Mains, R. E. (1993). The prohormone convertases PC1 and PC2 mediate distinct endoproteolytic cleavages in a strict temporal order during proopiomelanocortin biosynthetic processing. *J. Biol. Chem.* **268**, 1763-1769.

Journal of Cell Science

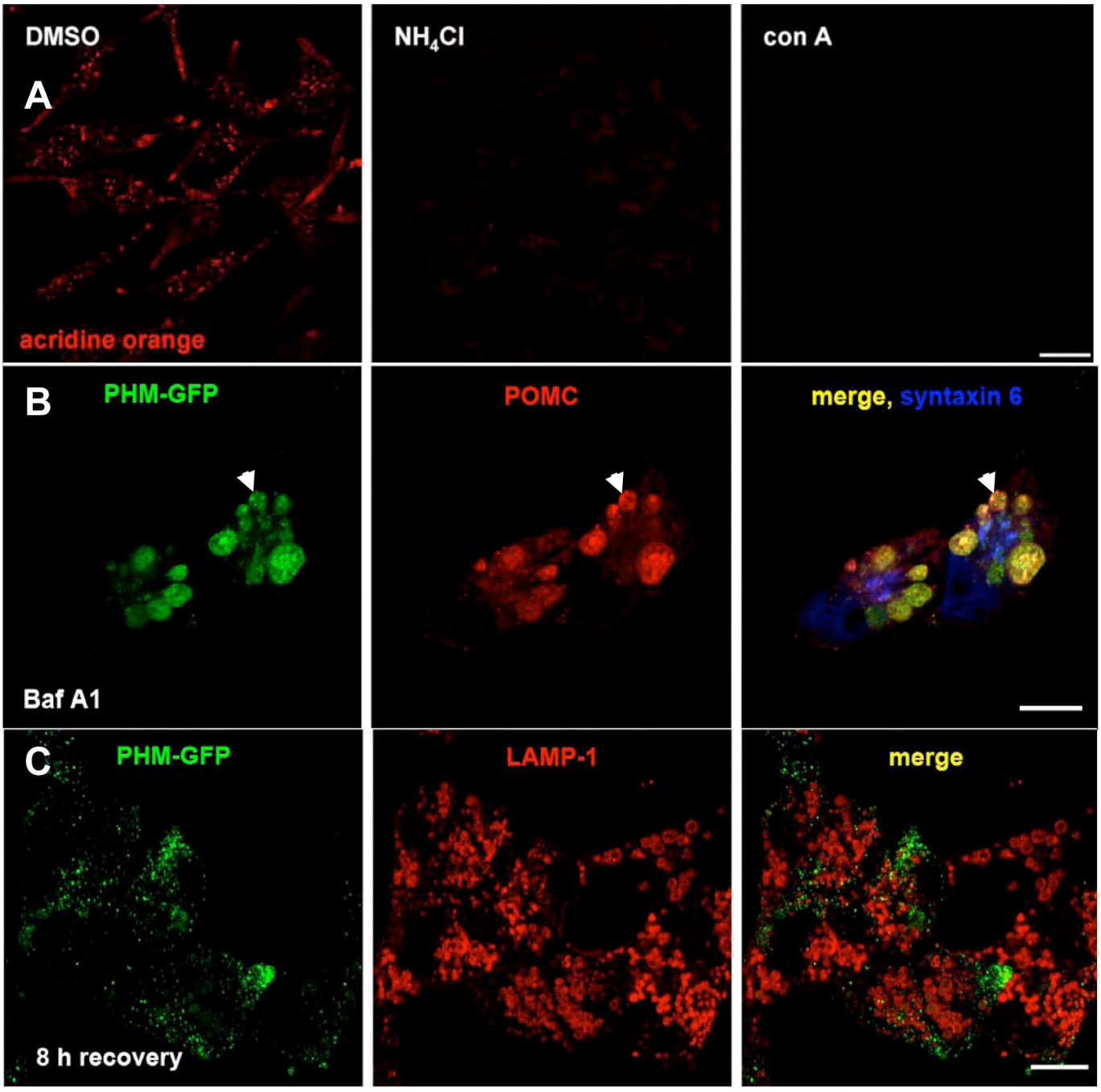
DMSO
A
acridine orange
NH4Cl
con A
B
PHM-GFP
POMC
merge, syntaxin 6
Baf A1
C
PHM-GFP
LAMP-1
merge
8 h recovery

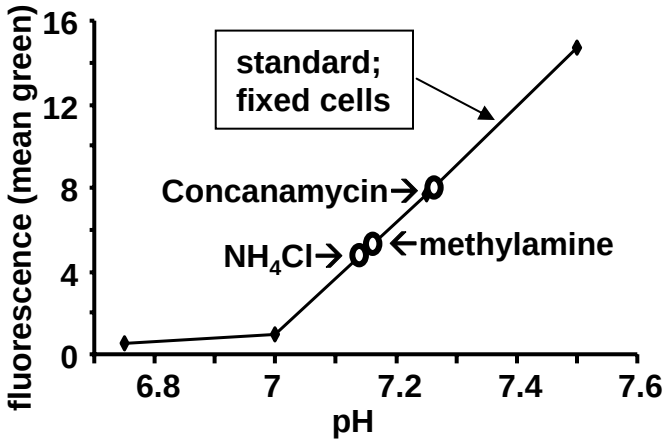
fluorescence (mean green)
16
12
8
4
0
6.8
7
7.2
7.4
7.6
pH
standard;
fixed cells
Concanamycin→
NH4Cl→
←methylamine

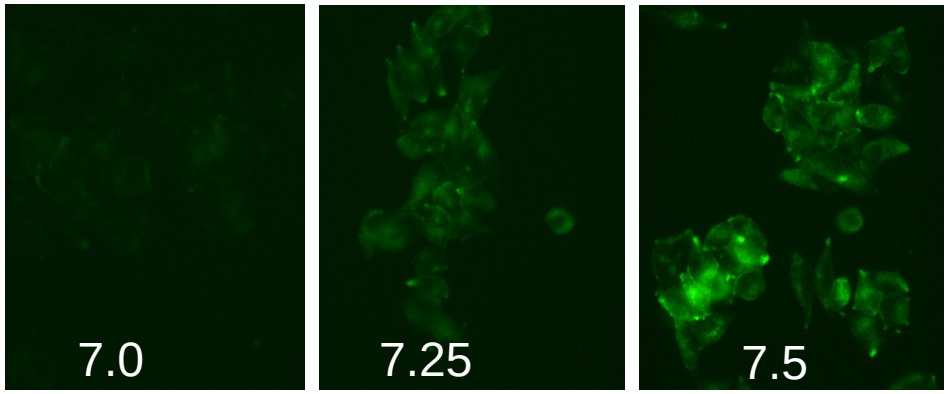
7.0
7.25
7.5

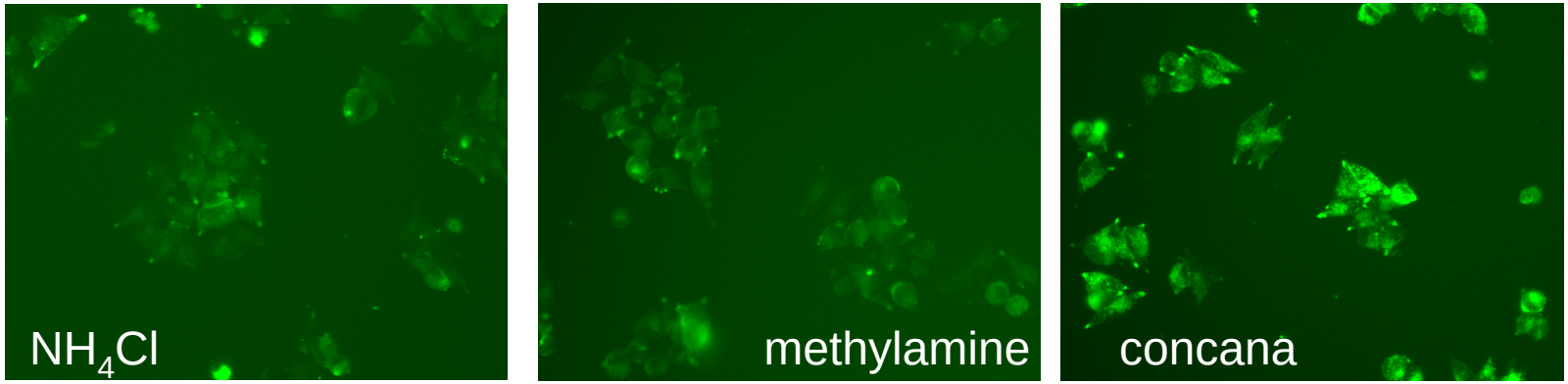
NH4Cl
methylamine
concana

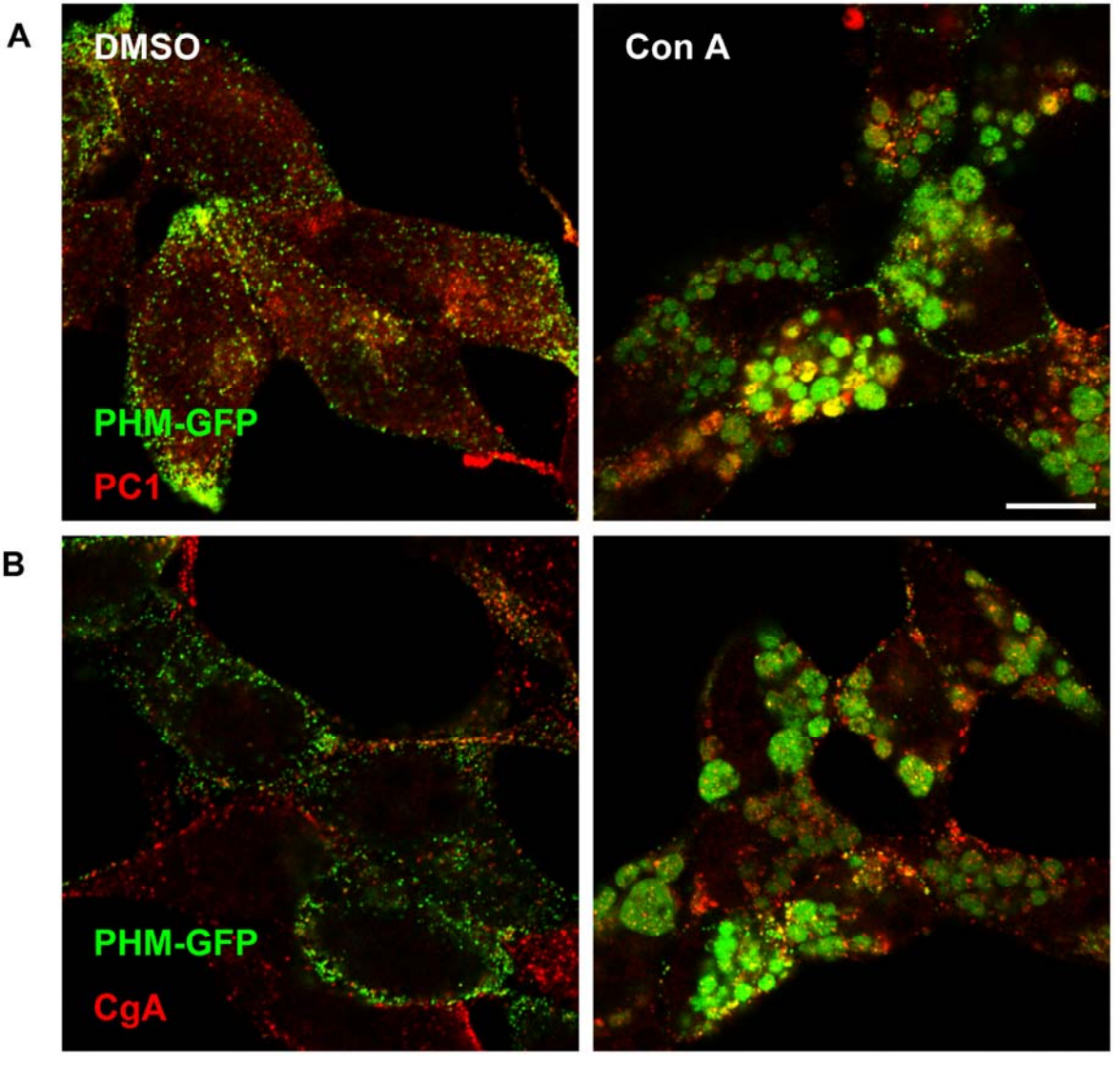
A
DMSO
Con A
PHM-GFP
PC1
B
PHM-GFP
CgA

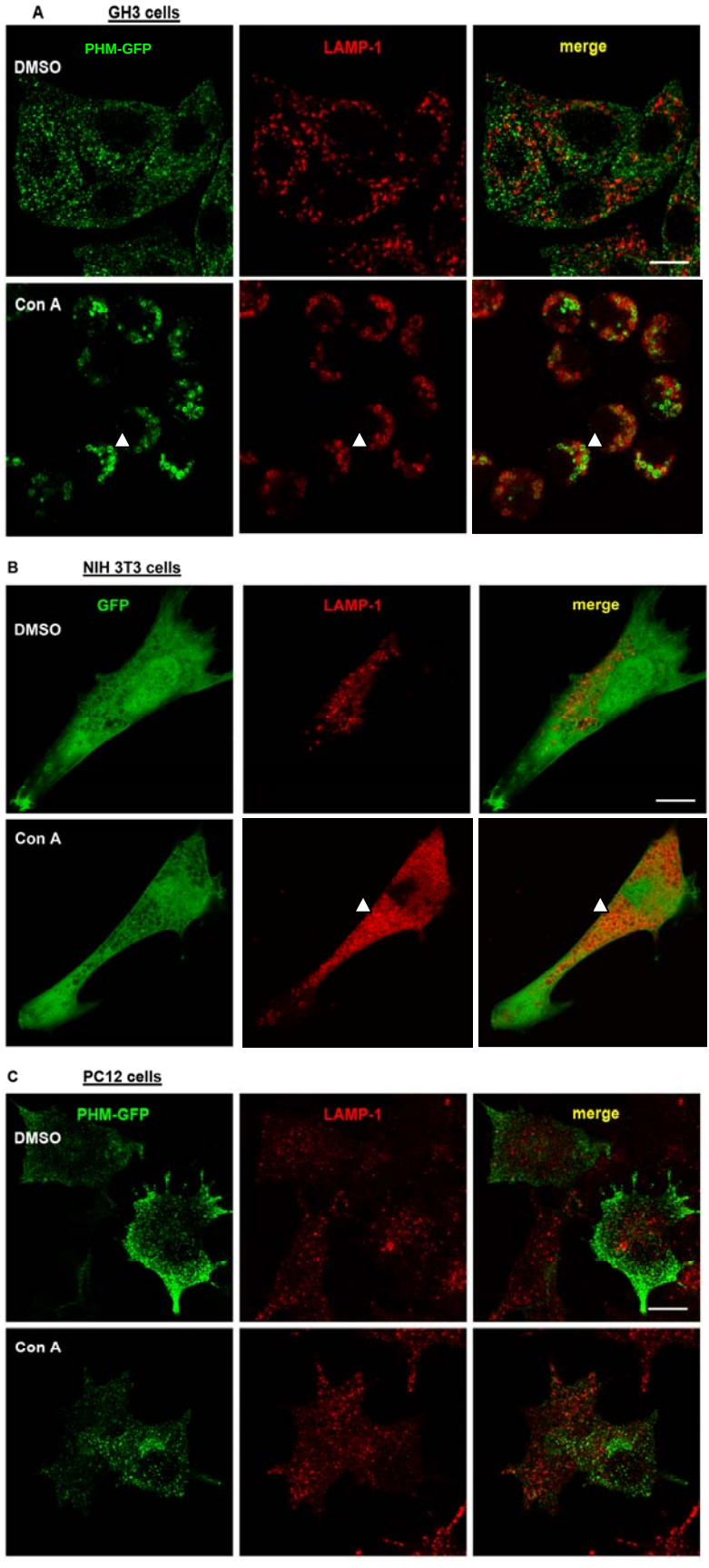
A
GH3 cells
PHM-GFP
LAMP-1
merge
DMSO
Con A
B
NIH 3T3 cells
GFP
LAMP-1
merge
DMSO
Con A
C
PC12 cells
PHM-GFP
LAMP-1
merge
DMSO
Con A

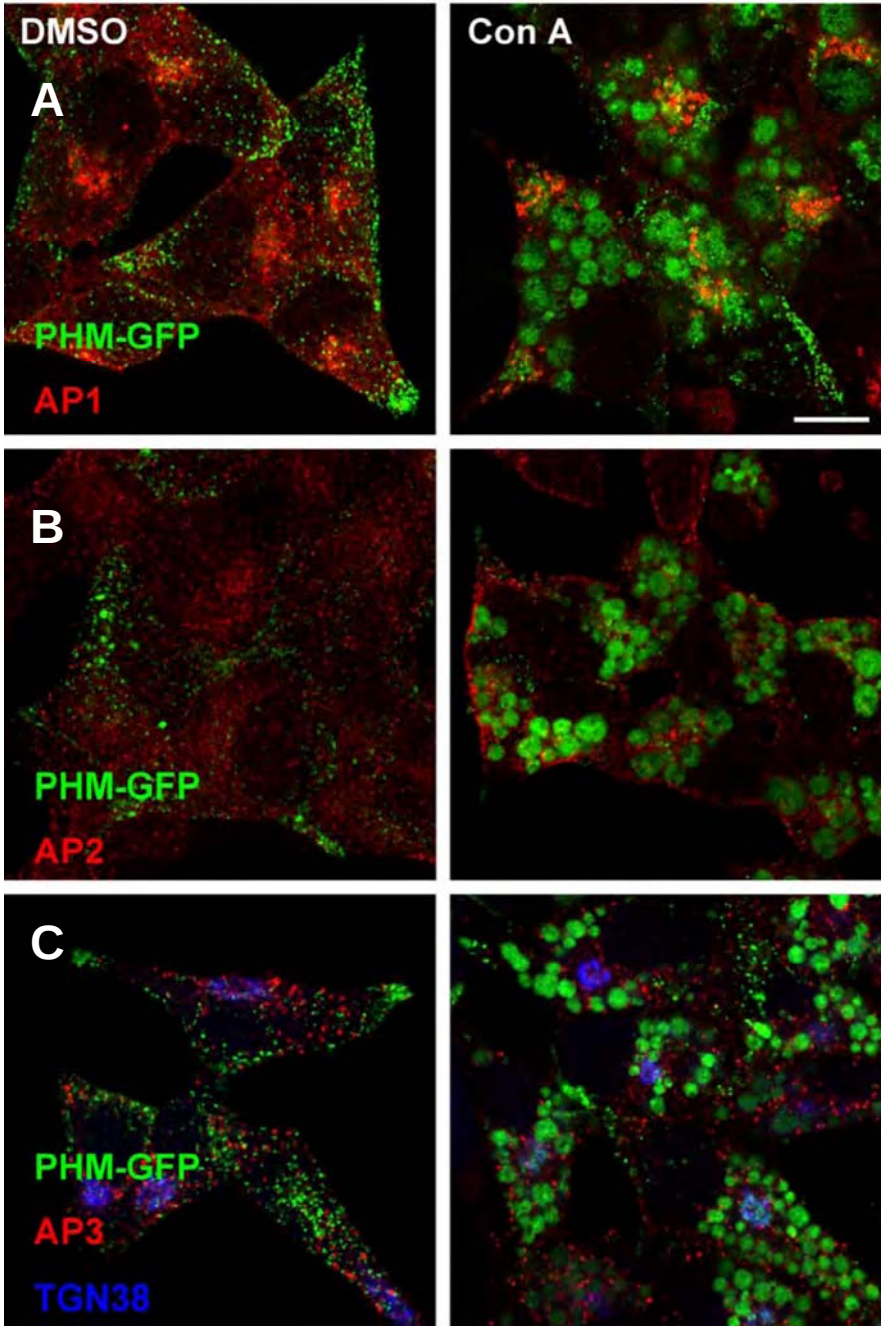
DMSO
Con A
A
PHM-GFP
AP1
B
PHM-GFP
AP2
C
PHM-GFP
AP3
TGN38

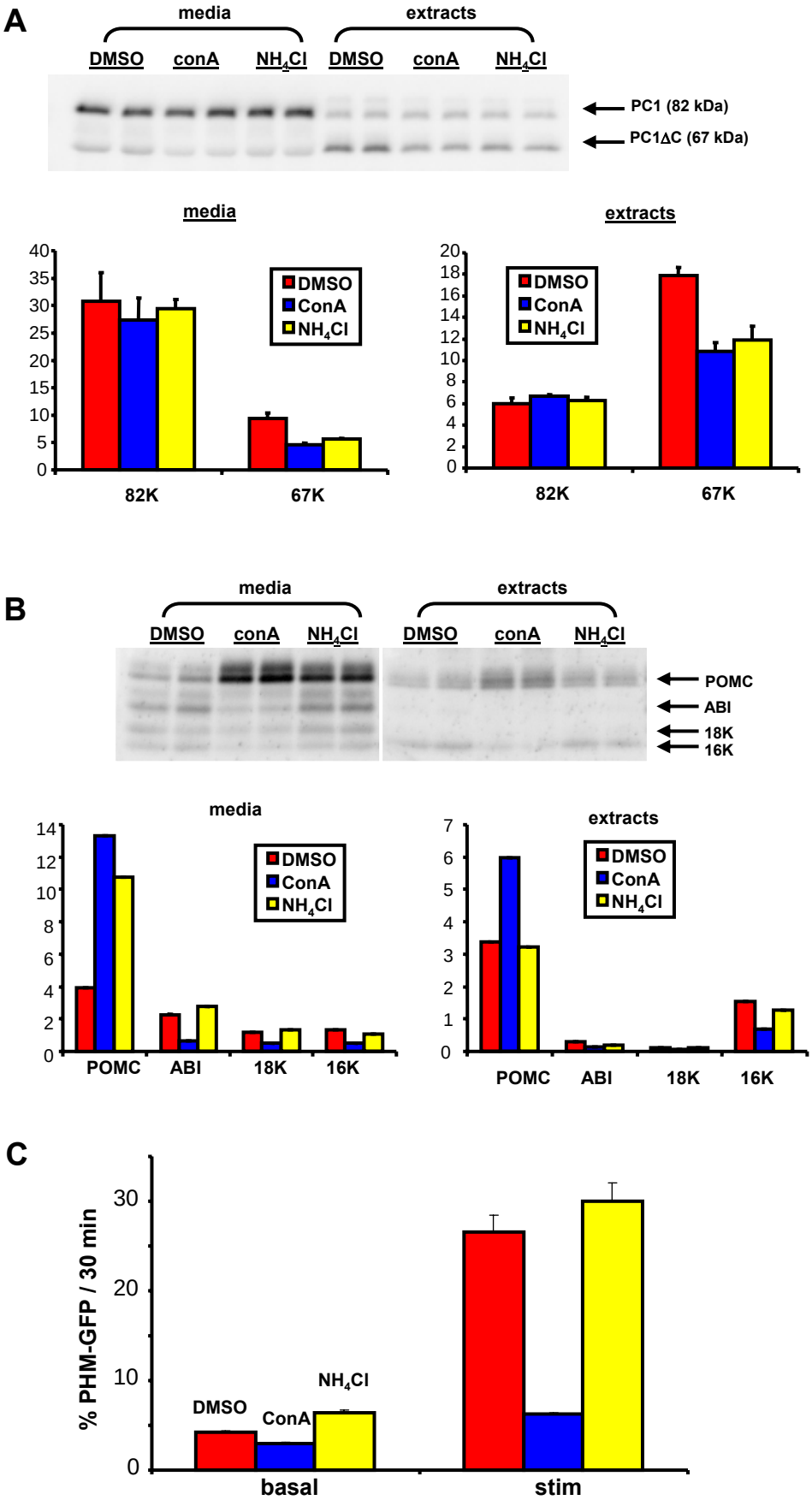
A
media
extracts
DMSO
conA
NH4Cl
DMSO
conA
NH4Cl
PC1 (82 kDa)
PC1ΔC (67 kDa)
media
extracts
DMSO
ConA
NH4Cl
82K
67K
B
media
extracts
DMSO
conA
NH4Cl
DMSO
conA
NH4Cl
POMC
ABI
18K
16K
media
extracts
POMC
ABI
18K
16K
C
% PHM-GFP / 30 min
DMSO
ConA
NH4Cl
basal
stim

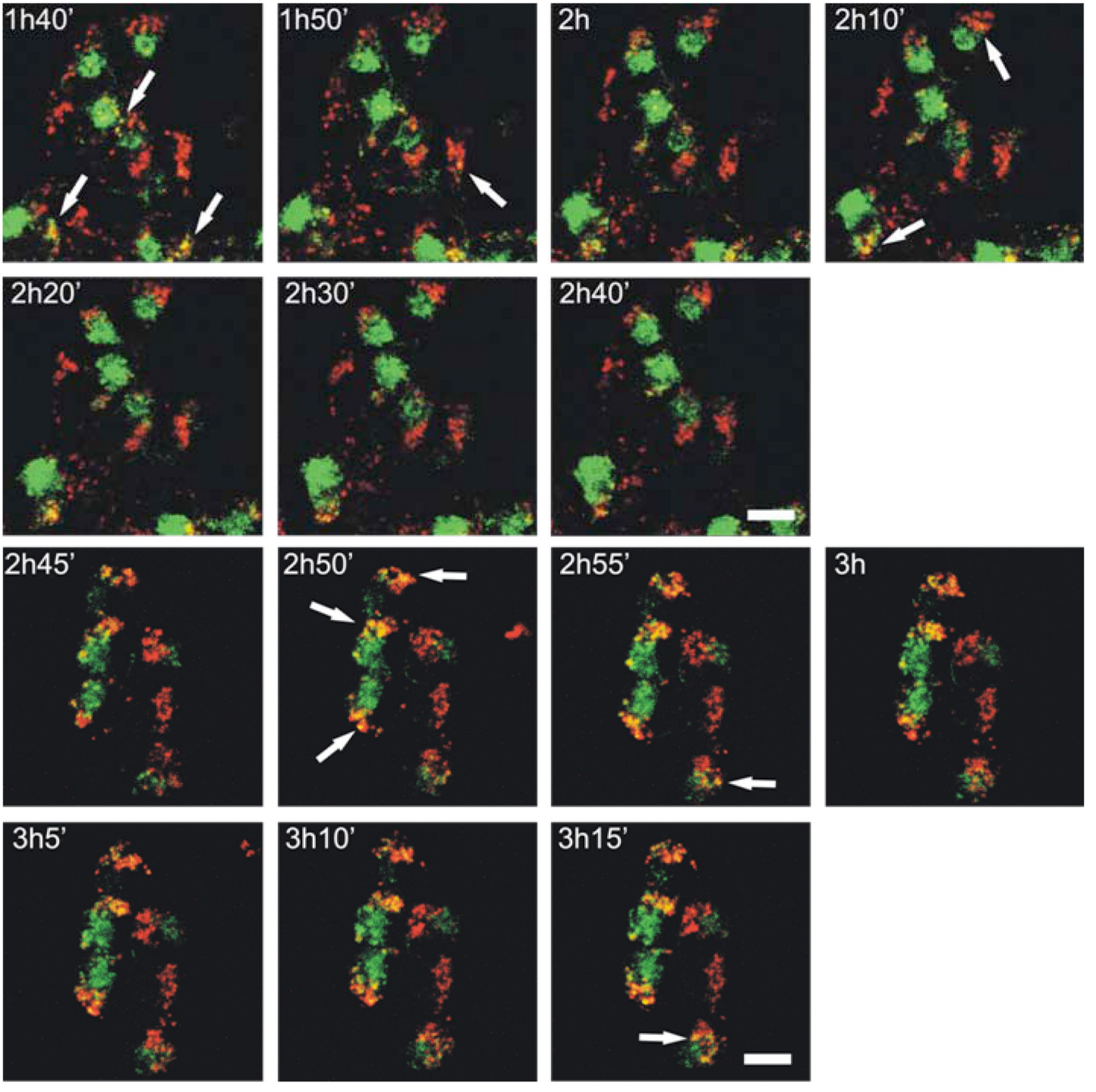
1h40'
1h50'
2h
2h10'
2h20'
2h30'
2h40'
2h45'
2h50'
2h55'
3h
3h5'
3h10'
3h15'

Table S1. shRNA sequences selected for insertion into pSIREN

Subunit	GenBank	Nucleotide sequence	Amino acids
V0-c	M64298.1	^{311}CCATCATCCCAGTGGTTAT^{329}	^{104}SIIPVVM^{110}
V0-c′=b=f255	NM_033617	^{255}GGCCTAGCAATTTCTCTGT^{273}	^{86}GLAISLS^{92}
V0-c′=b=f470	NM_033617	^{470}TGGCCATCGAAACTACCAT^{488}	^{158}GHRNYHA^{164}
V0-c′=b=f661	NM_033617	^{661}GGGTCATTGTTGCAATCCT^{679}	^{221}GVIVAIL^{227}
V0-a1	AF218249	^{343}CAGGAAGCTCTGAAGAGAA^{361}	^{115}QEALKRN^{121}
V0-a2	AF218252	^{350}AGCTGAGGAAGAACCTGTT^{368}	^{116}KLRKKLR^{123}
V1-A	NM_007508	^{518}GAGGAAGCGTGACTTACAT^{536}	^{173}RGSVTYI^{179}

After transfection, AtT-20 PHM-GFP cells were allowed to recover for 18-48 hours. Based on our experience with neurons expressing pSIREN shRNAs targeted to other transcripts, cells that express readily visible DsRed show sustained knockdown of the target protein (Ma et al., 2008). For the initial experiments with shRNAs targeted to the V0-c, V0-a1, V0-a2 and V1-A subunits of the V-ATPase, many cells expressing DsRed detached from the dish. The shRNAs targeted to the V0-c′=b=f subunit were better tolerated by AtT-20 cells, and all three shRNAs disrupted the cellular morphology in the TGN region to varying extents (Fig. 9).